Spatial Variation of In-Situ Stress Orientation Along the Hikurangi Subduction Margin: Insights from Borehole Image Logging

Effat Behboudi[1], David Daniel McNamara[2], Ivan Lokmer[3], Laura Wallace[4], and Demian M Saffer[5]

[1]School of Earth Sciences
[2]University of Liverpool
[3]University College Dublin
[4]GNS Science
[5]University of Texas at Austin

November 21, 2022

Abstract

Knowledge of the contemporary in-situ stress orientations in the Earth's crust can improve our understanding of active crustal deformation, geodynamic processes, and seismicity in tectonically active regions such as the Hikurangi Subduction Margin (HSM), New Zealand. The HSM subduction interface is characterized by varying slip behavior along strike, which may be a manifestation of variation in the stress state and the mechanical strength of faults and their hanging walls, or, alternatively, these variations in seismic behavior may generate variation in the stress state in space and time. In this study, we analyze borehole image and oriented four-arm caliper logs acquired from thirteen boreholes along the HSM to present the first comprehensive stress orientation dataset within the HSM upper plate. Our results reveal a NE-SW SHmax orientation (parallel to the Hikurangi margin) within the central HSM (Hawke's Bay region) which rotates to a WNW- ESE SHmax orientation (roughly perpendicular to the Hikurangi margin) in the southern HSM. This rotation of SHmax orientation spatially correlates with along-strike variations in subduction interface slip behavior, characterized by creep and/or shallow episodic slip events in the central HSM and interseismic locking in the southern HSM. Observed borehole SHmax orientations are largely parallel to maximum contraction directions derived from geodetic surface deformation measurements, suggesting that modern stress orientations may reflect contemporary elastic strain accumulation processes related to subduction megathrust locking.

E. Behboudi[1,2], D.D. McNamara[3], I. Lokmer[1,2], L. Wallace[4,5], and D. Saffer [5]

[1] Irish Centre for Applied Geosciences (iCRAG), University College Dublin, Republic of Ireland.

[2] School of Earth Sciences, University College Dublin, Republic of Ireland.

[3] Department of Earth, Ocean and Ecological Sciences, University of Liverpool, UK.

[4] GNS Science, New Zealand.

[5] University of Texas Institute for Geophysics, USA.

Corresponding author: Effat Behboudi (effat.behboudi@ucdconnect.ie)

Key Points:

- Maximum horizontal stress orientation varies along strike in the Hikurangi Subduction Margin upper plate
- Stress orientations reflect contemporary elastic strain accumulation processes related to subduction megathrust locking
- Stress orientations in the southern HSM are oblique to focal-mechanism stress suggesting the subduction interface is mechanically weak

Abstract

Knowledge of the contemporary in-situ stress orientations in the Earth's crust can improve our understanding of active crustal deformation, geodynamic processes, and seismicity in tectonically active regions such as the Hikurangi Subduction Margin (HSM), New Zealand. The HSM subduction interface is characterized by varying slip behavior along strike, which may be a manifestation of variation in the stress state and the mechanical strength of faults and their hanging walls, or, alternatively, these variations in seismic behavior may generate variation in the stress state in space and time. In this study, we analyze borehole image and oriented four-arm caliper logs acquired from thirteen boreholes along the HSM to present the first comprehensive stress orientation dataset within the HSM upper plate. Our results reveal a NE-SW S_{Hmax} orientation (parallel to the Hikurangi margin) within the central HSM (Hawke's Bay region) which rotates to a WNW-ESE S_{Hmax} orientation (roughly perpendicular to the Hikurangi margin) in the southern HSM. This rotation of S_{Hmax} orientation spatially correlates with along-strike variations in subduction interface slip behavior, characterized by creep and/or shallow episodic slip events in the central HSM and interseismic locking in the southern HSM. Observed borehole S_{Hmax} orientations are largely parallel to maximum contraction directions derived from geodetic surface deformation measurements, suggesting that modern stress orientations may reflect contemporary elastic strain accumulation processes related to subduction megathrust locking.

Plain Language Summery

Movement along faults at tectonic plate boundaries can cause changes in the orientations of the forces, known as stress, that make them move. Such changes may help us explain how deformation at the surface occurs when these faults move, the way fluid moves along these faults, and why different types of earthquakes occur on these faults. The Hikurangi Subduction Margin, New Zealand's largest and most hazardous plate boundary fault, shows a variety of deformation and earthquake types that occur in the over-riding plate which may be linked to stress orientation. In this study, we found that variability in the stress orientations within the upper plate of Hikurangi Subduction Margin matches areas where we see different earthquake types occurring, and observed patterns of surface deformation. We suggest that stress orientations reflect the accumulation and release of strain caused by subduction at the HSM.

1 Introduction

In-situ stress measurements can provide important insights into stress states at global and localized scales, the geomechanical state of earthquake-hosting faults, shear traction on faults, and processes of stress accumulation and release on plate boundary faults. Such measurements also assist with understanding how crustal stresses relate to strain observed geodetically and geologically (e.g., Zoback et al., 1987; Magee & Zoback, 1993; Townend & Zoback, 2006; Byrne et al., 2009; Chang et al., 2010; Lin et al., 2013, 2016; Brodsky et al., 2017). Earthquake occurrence and many earthquake rupture characteristics are partly dependent on the shear to normal stress ratio, which is a function of the relative magnitude of in-situ principal stresses, the orientation of the fault plane with respect to the orientation of the principal stress orientations, pore pressure, and fault plane friction coefficients (Jaeger et al., 2007; Schellart & Rawlinson, 2013; Vavryčuk, 2015). Additionally, earthquakes can redistribute stress and change both shear and normal stress on adjacent fault planes and surrounding rocks either statically (a shift in the stress state from before to after the earthquake) or dynamically (oscillating stress changes that occur with the passage of seismic waves) (Stein, 1999; Seeber & Armbruster, 2000; Hardebeck, 2004; Ma et al., 2005; Lin et al., 2007, 2016; Hardebeck & Okada, 2018).

The Hikurangi Subduction Margin (HSM), on the east coast of the North Island of New Zealand (Figure

1a), experiences strong along-strike variations in megathrust slip behaviour, ranging from deep interseismic locking (and stress accumulation) beneath the southern North Island, to episodic slow slip events (SSEs) and creep at the northern and central HSM (Figure 1b). Creep and shallow (<15 km depth) SSEs lasting for 2-3 weeks recur every 18-24 months offshore of the northern and central HSM (Wallace & Beavan 2010; Wallace, 2020; Figure 1b). Deep (>25 km), long-term (>1 year) slow slip events occur approximately every ~5 years at the southern HSM (Wallace & Beavan 2010), just down-dip of a portion of the plate interface that is strongly locked and accumulating stress likely to be released in a future great earthquake (Mw > 8.0). Despite the recognized importance of in-situ stress states along active subduction zones in understanding strain accumulation and release, few studies have been undertaken to directly estimate stress magnitudes in these settings (Chang et al., 2010; Huffman & Saffer, 2016; Lin et al., 2010, 2013, 2016; Malinverno et al., 2016; Brodsky et al., 2017; McNamara et al., 2021).

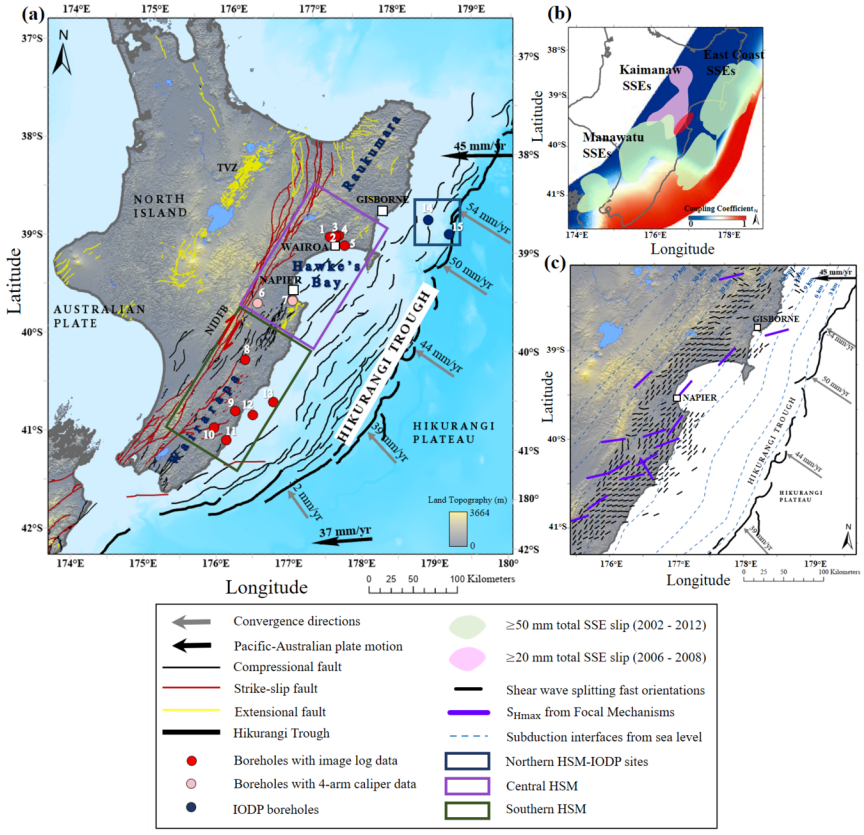

Figure 1. (a) Tectonic setting of East Coast of North Island, New Zealand. Fault traces from Barnes et al., (2010), Langridge et al, (2016), Mountjoy and Barnes (2011), and Pedley et al., (2010). Black arrows indicate the long-term motion of the Pacific relative to Australian Plate from DeMets et al., (1994) and grey arrows show shortening rates at the Hikurangi Trough from Wallace et al. (2012). (b) Interseismic coupling based on campaign GPS velocities (1995–2008), shown in terms of coupling coefficient (Wallace et al. 2012a). Green and pink shaded regions represent the cumulative slow slips in 2002 and 2012 (Wallace et al., 2012a) and SSEs beneath the Kaimanawa ranges in 2006 and 2008 (Wallace & Eberhart-Phillips, 2013; Wallace, 2020). Area of possible locked patch between the East Coast and Kaimanaw SSEs is shaded in red. (c) Map showing S_{Hmax} orientations from focal mechanisms (Townend et al., 2012) and shear wave splitting fast orientations (Illsley-Kemp et al., 2019). Boreholes are numbered 1: Makareo-1, 2: Kauhauroa-2, 3: Waitahora-1, 4: Kauhauroa-5, 5: Tuhara-1A, 6: Kereru -1, 7: Whakatu-1, 8: Ngapaeruru-1, 9: Te Mai-2, 10: Rauni-2, 11: Orui-1A, 12: Titihaoa-1, 13: Tawatawa-1, 14: U1519A, and 15: U1518B. Abbreviations:

NIDFB, North Island Dextral Fault Belt; TVZ, Taupo Volcanic Zone.

To date, several studies have been carried out to determine the contemporary in-situ stress patterns along the East Coast of the HSM. Analysis of earthquake focal mechanism solutions reveal that S_{Hmax} orientations in the crust ([?]60 km depth) change from NE-SW (roughly margin-parallel; Figure 1c) in the northern and central Hikurangi margin to a more margin-oblique, ENE-WSW orientation, sub-parallel to Pacific/Australia relative plate motion, further south (Figure 1c). These measurements are largely from earthquakes within the subducting slab most located at depths >25 km depth (Townend et al., 2012). In contrast, the seismic anisotropy fast orientations determined from shear wave splitting methods that sample the upper ~40 km (Figure 1c) suggest a dominant S_{Hmax} orientation of NE-SW for most of the HSM forearc (generally margin-parallel), while the northern HSM forearc displays variable fast orientations, with a more dominant ENE-WSW inferred S_{Hmax} orientation (Illsley-Kemp et al., 2019). Shallow (<3km) S_{Hmax} orientations have been determined from limited analysis of borehole image logs from boreholes drilled onshore and offshore HSM (Heidbach et al., 2018; Lawrence, 2018; Griffin, 2019; Griffin et al., 2021; McNamara et al., 2021). Analysis of borehole image data from four onshore boreholes show NE-SW to ENE-WSW S_{Hmax} orientations in the central HSM (Heidbach et al., 2018; Lawrence, 2018;), and an E-W to NW-SE SHmax orientation is determined from two borehole image logs in the southern HSM (Heidbach et al., 2018; Griffin, 2019; Griffin et. al, 2021). Boreholes offshore the northern HSM drilled as part of the International Ocean Discovery Program (IODP) Expeditions 372 and 375 show an E-W S_{Hmax}orientation close to the Hikurangi trench, and a NW-SE S_{Hmax} orientation in the offshore forearc (McNamara et al., 2021), indicating strong variations in stress orientations across the forearc.

In this study, we provide a detailed analysis of S_{Hmax}orientations from stress related drilling-induced borehole failures, and assess their variability within the upper plate of the HSM. We analyze six borehole image and oriented four-arm caliper logs (not previously used for stress orientation studies), and provide a reanalysis of the seven borehole image logs investigated in Heidbach et al. (2018), Lawrence (2018), Griffin (2019), and Griffin et al. (2021) with a focus on acquiring higher resolution measurements (length, width, orientation) of induced borehole features. We then discuss spatial variations in contemporary S_{Hmax} orientations and their relationship to far-field stresses and long-term patterns of tectonic deformation, and their potential links to along-strike variations in subduction megathrust slip behavior.

2 Geological Setting

The Hikurangi Subduction Margin (HSM) lies along the Pacific-Australian plate boundary at the southern end of the Tonga-Kermadec Trench, off the east coast of the North Island, New Zealand (Figure 1a). The Hikurangi Subduction Margin accommodates westward subduction of the Hikurangi Plateau (a Cretaceous large igneous province) beneath the continental crust of North Island at the Hikurangi Trough (Davy, 1992). The Hikurangi Plateau is ~10-15 km thick and transitions to a more typical 5-7 km thick oceanic plate further north at the Kermadec Trench (Davy et al., 2008; Davy, 1992; Ghisetti et al., 2016; Mochizuki et al., 2019). The southern termination of the HSM is located somewhere beneath New Zealand's northeastern South Island, where oblique convergence is transferred to the Marlborough Fault System and Alpine Fault in the South Island (Barnes et al., 1998; Little & Roberts, 1997).

Three major tectonic phases during the Neogene to present-day have been identified: 1) an early to middle Miocene compressional stage that resulted in extensive reverse faulting, folding, and tectonic uplift along the margin (Chanier et al., 1999; Barnes et al., 2002; Bailleul et al., 2013); 2) a mixed compressional and extensional stage from the mid-Miocene to early Pliocene resulting in widespread compressional tectonics and localized subsidence and normal faulting in the inner portion of the subduction wedge (Hawke's Bay region) (Barnes et al., 2002); 3) a compressional stage associated with and structural inversion of listric thrust faults and folds during the Quaternary and rapid, late Quaternary uplift of the Coastal Ranges, Axial Ranges, and Raukumara Peninsula (Beanland & Haines, 1998; Nicol et al., 2002, 2007; Nicol & Beavan, 2003; Bailleul et al. 2013). Late Quaternary extensional faulting in the Raukumara Peninsula is likely the result of gravitational collapse due to rapid uplift (Berryman et al., 2009; Pettinga, 2004; Walcott, 1987).

Neogene to present tectonic deformation across the HSM is complex and includes contributions from shortening associated with subduction at the Hikurangi Trough, clockwise rotation of the East Coast forearc, strike-slip faulting along the North Island Dextral Fault Belt (NIDFB), and back-arc extension in the Taupo Volcanic Zone (TVZ) (Beanland & Haines, 1998; Wallace et al., 2004; Figure 1a). The East Coast forearc has rotated for at least the last few Myr at rate of 3°–4°/Myr relative to the Australian plate (Nicol et al. 2007). This rotation results in back-arc rifting in the central North Island's Taupo Volcanic Zone (TVZ), transpression in the southern North Island, and creates a large along-strike change in convergence rate at the Hikurangi Trough, from 20 mm/year in the south to 60 mm/year at the northern Hikurangi Trough (Wallace et al. 2004; Figure 1a). Wallace et al. (2004) suggest that an along-strike change from subduction of the large igneous province (Hikurangi Plateau) at the Hikurangi Trough, to normal oceanic crust along the Kermadec Trench exerts a torque on the forearc, producing clockwise rotation of the eastern North Island. Overall, relative motion between the Pacific and Australian plates occurs through this region at ~40 mm/yr, and is oblique to the orientation of the plate boundary. The oblique relative motion is partitioned into a margin-perpendicular component and a margin-parallel component. The margin-perpendicular component occurs along the Hikurangi subduction interface and provides a NW-SE shortening which is accommodated via the subduction interface and active thrust faults within the accretionary wedge and overriding plate (Barnes et al., 1998; Nicol and Beavan, 2003). The margin-parallel component is largely accommodated by a combination of right-lateral strike-slip on the North Island Dextral Fault Belt (NIDFB) and vertical-axis clockwise rotation of the North Island forearc (Beanland & Haines, 1998; Nicol et al., 2007; Wallace et al., 2004).

3 Data and Methodology

We analyze borehole image logs acquired from eleven boreholes using a range of tools including; the Schlumberger Fullbore Formation Microimager (FMI; Figure 2a) and Oil Based Mud Imaging tool (OBMI), Baker Atlas Simultaneous Acoustic and Resistivity Imager (STAR), Tiger Energy Services Acoustic Formation Imaging Technology (AFIT; Figure 2b), and two orientated four-arm caliper logs (Figure 2c). The tool types and their borehole wall coverage for each borehole are summarized in Table 1.

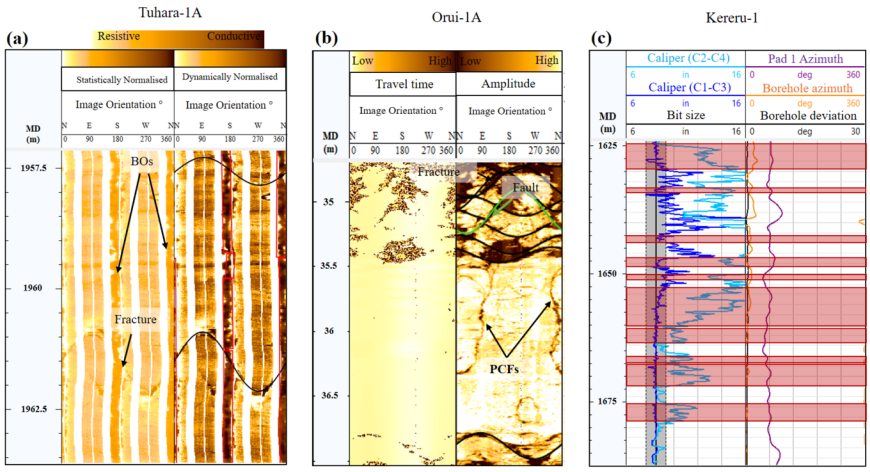

Figure 2. (a) Statically and dynamically normalized resistivity image log (FMI) showing borehole breakouts and natural fractures in borehole Tuhara-1A, (b) Dynamically normalized travel time and amplitude images from an acoustic image log (AFIT) acquired in Orui-1A borehole showing petal centerline fractures (PCFs), natural fractures, and a fault (observable offset of other geological features across a natural fracture). (c) Plot of an oriented four-arm caliper log (C1-C3 and C2-C4) from borehole Kereru-1. The 10% tolerance of bit size (black line) is shown as a grey shaded zone, plotted next to pad 1 azimuth and borehole orientation information showing caliper enlargement indicative of the presence of a borehole breakout.

Image log acquisition, data processing, and quality assessment is performed on all image logs, the details of which are documented in the supplemental information (Text S1 & S2).

From the borehole image logs, we identify stress-induced borehole failures, including borehole breakouts (BOs; Figure 2a & 2c), drilling-induced tensile fractures (DITFs), and petal-centerline fractures (PCFs; Figure 2b). BOs and DITFs are well-known indicators of horizontal in-situ stress orientations in vertical to semi-vertical boreholes, in which it is assumed one of the principal stresses is the vertical stress (S_v). BOs and DITFs develop parallel to the contemporary minimum (S_{hmin}) and maximum (S_{Hmax}) horizontal stresses respectively (Bell, 2003; Bell & Gough, 1979; Aadnoy & Bell, 1998). In such cases, BOs and DITFs can also be used to determine S_{Hmax} orientations in boreholes deviated $\geq$20 as long as corrections are applied to address the impact of vertical stress (S_v) on their development (Peška & Zoback, 1995). BOs form as enlargements of the borehole diameter on opposite sides of the borehole wall where the circumferential hoop stress, induced by non-uniform horizontal principal stress magnitudes, is large enough to exceed the rock strength (Bell & Gough, 1979; Zoback, 2007). Borehole breakouts typically appear on resistivity image logs as a pair of wide, conductive (in water-based mud) or resistive (in oil-based mud, such as OBMI tool; King et al., 2010) zones. In acoustic televiewer logs, they appear as low amplitude, out-of-focus zones (Figure 2a). In both types of logs, BOs are located ~180° from each other around the circumference of the borehole wall. BOs often correlate with borehole enlargement and associated large caliper values as the result of the borehole failure (Figure 2c; Tingay et al., 2008). Oriented four-arm caliper data is also used to infer the presence of BOs along boreholes. To reliably distinguish BOs from other non-stress related features that affect borehole shape, such as keyseats and washouts, we apply the criteria presented by Reinecker et al., (2003).

DITFs develop on the borehole wall where there is a significant difference between the two horizontal principal stress magnitudes and the local stress concentrations around the borehole wall lead to hoop stresses that overcome the tensile strength of the rock (Brudy & Zoback, 1999; Zoback, 2007; Barton & Moos, 2010). DITFs typically appear as narrow, conductive (on resistivity image logs) or low amplitude and longer travel time (on acoustic image logs) pairs, ~180° from each other around the circumference of the borehole wall. DITFs are generally parallel or slightly inclined to the borehole axis in vertical to semi-vertical boreholes (Barton et al., 1998; Bell, 2003; Tingay et al., 2008; Rajabi et al., 2016a, 2016b). In this study, all BOs and DITFs are reported as individual feature length and width, such that a single BO or DITF measurement does not span a number of separate individual BOs or DITFs, similar to what has been done in previously analyzed HSM image logs (Lawrence, 2018; Griffin, 2019). This is an important aspect of quantifying induced features from borehole image logs because geological properties, such as varying strength associated with variably bedded lithologies, impact the development and growth (both width and length) of borehole breakouts (Kingdon et al., 2016; Fellgett et al., 2019). It is also important to capture each induced feature individually for accurate statistical considerations of borehole stress orientations.

PCFs are induced fractures that form within the bedrock ahead of the drill bit in response to stress concentrations at the bottom of the borehole during drilling, and propagate inward towards the borehole (Li & Schmitt, 1998; Davatzes & Hickman, 2010; Wenning et al., 2017). PCFs appear as conductive (resistivity image logs) or low amplitude (acoustic image logs) partial sinusoids that merge into discontinuous borehole axial centerline fractures (Figure 2b; Kulander et al., 1990). The average of the centerline fracture orientations or dip orientation of the partial sinusoids of a PCF is parallel to the orientation of S_{hmin} (Davatzes & Hickman, 2010). In contrast to the DITFs, the centerline portions of PCFs are often less than 180° apart from each other around the circumference of the borehole wall.

Finally, we use the A–E World Stress Map (WSM) quality ranking system and circular statistical analysis for stress orientation indicators (Heidbach et al., 2016). The borehole locations, image log intervals, S_{Hmax} orientation mean, standard deviation, and the quality classification are based on the length-weighted method (Heidbach et al., 2016) for individual boreholes are summarized in Table 1 and Table 2.

4 Results

4.1 Central HSM (Hawke's Bay region)

A total of 810 BOs with a combined length of 454 m are identified from borehole image logs and oriented four-arm caliper logs acquired in Kauhauroa-2, Kauhauroa-5, Makareao-1, Tuhara-1A, Kereru-1, and Whakatu-1 boreholes in the Central HSM region (Figure 3; data set 1; see Fig. 5 for the borehole locations and names). Using only BOs from boreholes with B-C quality rankings (following the WSM criteria), and so more likely to display far-field stress orientation measurements, a dominant 157°/337° ± 18° orientation is observed, indicating a NW-SE S_{hmin} orientation, from which we infer an S_{Hmax} orientation of 067°/247° (ENE-WSW) (Figure 3). The only exception is borehole Whakatu-1 (WSM D quality ranking), in the southeast area of the central HSM, which shows a dominant BO orientation of 054°/234° ±13° (NE-SW), from which we infer a NW-SE S_{Hmax} orientation (144°/324°) (Table 1; Figure 3). 2 DITF pairs are observed in boreholes Kauhauroa-5 and Tuhara-1A with mean S_{Hmax} orientation of 020°/195° (NNE-SSW) and 079°/263° (ENE-WSW), respectively (Figure 3). No BOs, DITFs, or PCFs are observed in Waitahora-1 borehole from OBMI image logs (this image log only provided ~37% coverage of borehole wall) or from oriented four-arm caliper data.

Table 1. *Stress Indicators From Analysis of Borehole Image Logs and Oriented Four-Arm Caliper Data in the Central HSM, New Zealand.*

	Borehole ID	Year	Max borehole Deviation (°)	Tool name	Borehole coverage (%)	Image interval (m MD)	Feature type	Number	Mean S_{Hmax}	S.D (°)	Total length (m)	Q
Northern central HSM	**Kauhauroa-2**	1998	1.78	FMI^{TM}	75	1824.2-2138.5	BO	52	069°/249°	15	24	C
	Kauhauroa-5	1999	2.57	FMI^{TM}	75	1277.1-1750.2	BO DITF	260 1	052°/232° 020°/195°	16 -	75 3.1	B
	Makareo-1	1998	2.65	FMI^{TM}	52	485.2-939.7	BO	140	058°/238°	20	60	B
	Tuhara-1A	2000	7.64	FMI^{TM}	75	1708-2148	BO DITF	334 1	71°/251° 079°/263°	15 -	239 0.16	B
Southern central HSM	**Kereru-1**	1996	1	4-arm caliper	75	1622-1920	BO	16	79°/259°	14	43	C
	Whakatu-1	2000	1.53	4-arm caliper	75	525-1400	BO	8	144°/324°	11	13	D

Note. S_{Hmax} azimuth means, standard deviations (S.D.), and data quality ranking are calculated according to World Stress Map conventions (Heidbach et al., 2016).

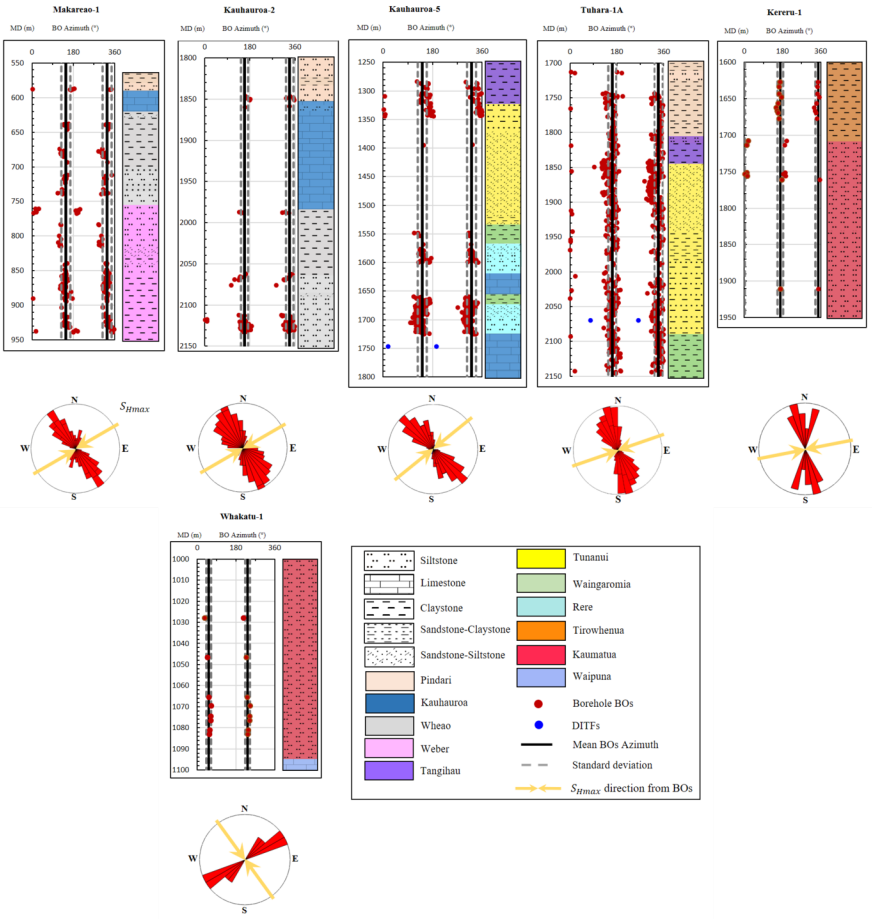

Figure 3. Graph of BO azimuths (red dots), DITF azimuths (blue dots), and stratigraphy column against measured depth (m MD) for boreholes at the central HSM. Mean BO azimuths and the standard deviation for individual borehole are plotted in black and dashed grey lines respectively. Bi-directional rose diagram of breakout orientations for each borehole is shown below BO panels.

4.2 Southern HSM

A total of 1517 BOs with a combined length of 520 m are identified from borehole image logs in boreholes Ngapaeruru-1, Rauni-2, Titihaoa-1, Tawatawa-1, Te Mai-2, and Orui-1A boreholes (Figure 4; data set 1). For borehole stress data with a WSM quality ranking of B-C (Ngapaeruru-1, Tawatawa-1, and Ranui-2) we observe an S_{hmin} orientation of 016°/196° ± 21° (NNE-SSW) from which we infer an S_{Hmax} orientation of 106°/286° (WNW- ESE) (Figure 4). BOs in boreholes Ngapaeruru-1, Tawatawa-1, Te Mai-2, and the shallow (<1130 m MD) interval of Ranui-2 show a consistent WNW-ESE S_{Hmax} orientation (Figure 4), whereas BOs measured in boreholes Titihaoa-1, the deeper (>1130 m MD) imaged interval of Ranui-2, and Orui-1A provide dominantly NW-SE S_{Hmax} orientations (Figure 4). Our reanalysis of BOs from borehole Ranui-2 suggest a 51° clockwise S_{Hmax}orientation rotation from E-W (094°/274° ± 17°) in the shallower imaged depth interval (842-1130 m MD) to NW-SE (145°/325° ± 16°) in the deeper imaged interval (1130-1422 m MD) (Table 2) that was first reported by Griffin (2019).

Table 2. *Stress Indicators From Analysis of Borehole Image Logs in the Southern HSM, New Zealand.*

	Borehole ID	Year	Max borehole deviation (°)	Tool name	% Borehole surface coverage	Image interval (m MD)	Feature type	Number	Number	Mean S_{Hmax}	S.D (°)	T l (
Southern HSM	**Ngapaeruru-1**	2013	11.2-17.78	FMI^{TM}	75	970-1417	BO	282	112 °/292°	112 °/292°	12	6
	Rauni-2*	2012	8.1-25.4	FMI^{TM}	80	839-1130 1130-1422	BO BO	390	94°/274° 145°/325°	94°/274° 145°/325°	17 16	5
	Te Mai-2	2011	2.4	AFIT^{150}	100	35-147.5	BO	2	109°/289°	109°/289°	8	0
	Orui-1A	2011	1.6	AFIT^{150}	100	6.7-114.5	BO PCF DITF	4 1 1	155°/335° 125° 133/295°	155°/335° 125° 133/295°	11 - -	0 0
	Titihaoa-1	1994	2.3	FMI^{TM}	75	1983-2741	BO	14	152°/332°	152°/332°	10	7
	Tawatawa-1	2004	2.9	STAR	75	750-1540	BO	825	103°/283°	103°/283°	14	3

Note. S_{Hmax} azimuth means, standard deviations (S.D.), and data quality ranking are calculated according to World Stress Map conventions (Heidbach et al., 2016). *Measured stress feature orientatioind are not corrected for borehole deviations$\geq$ 20.

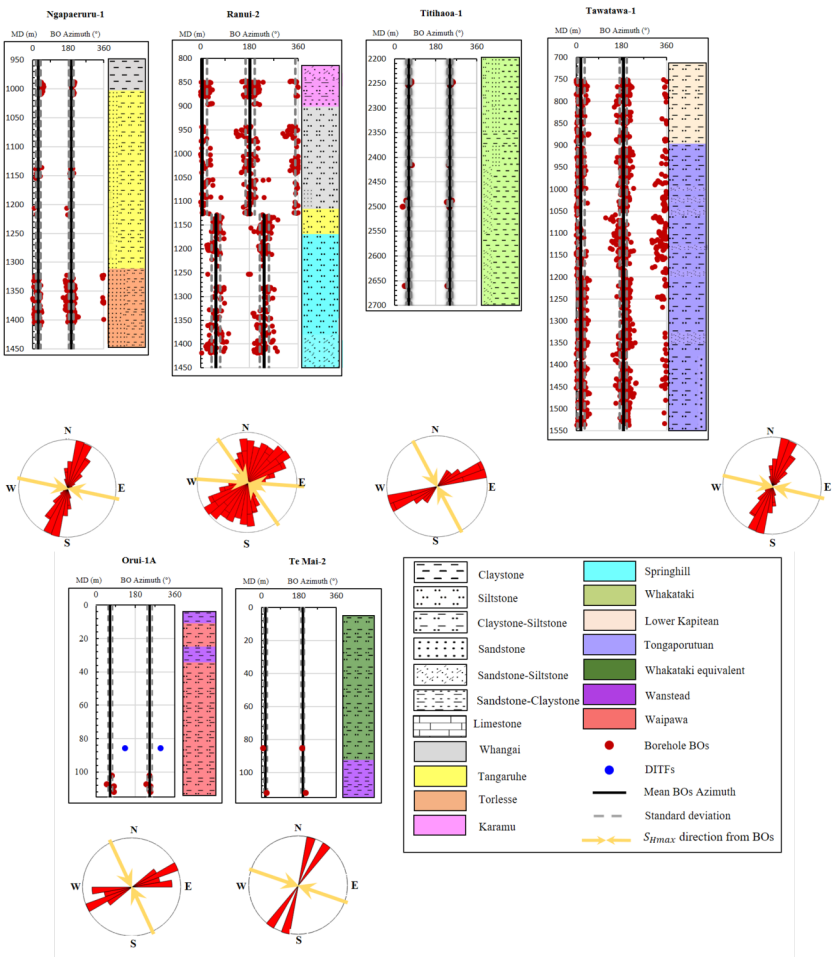

Figure 4. Graph of BO azimuths (red dots), DITF azimuths (blue dots), and stratigraphy column against measured depth (m MD) for boreholes at the southern HSM. Mean BO azimuths and the standard deviation for individual borehole are plotted in black and dashed grey lines respectively. Bi-directional rose diagram of breakout orientations for each borehole is shown below BO panels.

5 Discussion

Our results show that the contemporary S_{Hmax}orientations in the upper plate of the HSM change from dominantly NE-SW, parallel to the subduction margin, within the central HSM to WNW-ESE/NW-SE within the southern HSM (Wairarapa region), roughly perpendicular to the subduction margin (Figure 5). This along-strike rotation in HSM S_{Hmax} orientations may be explained in a few ways; 1) HSM kinematics, 2) long-term tectonic deformations, and 3) lateral variations in basement topography.

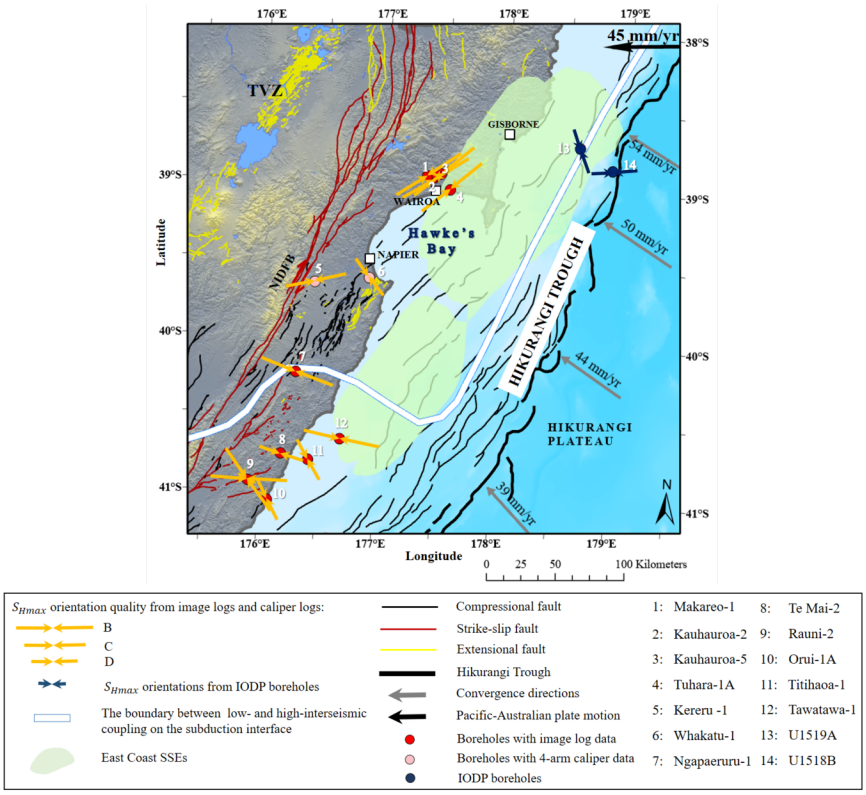

Figure 5. Map of S_{Hmax} at the East Coast of North Island determined from borehole Breakouts in (orange arrows) and IODP borehole image analysis from McNamara et al., 2021 (blue arrows). Green shaded region represents the East Coast cumulative slow slip (Wallace et al., 2012a). Active faults (normal faults: yellow; strike slip: red; reverse fault: black) traces from Litchfield et al. (2014) and Langridge et al, (2016). The bold black line shows the Hikurangi Through. Black arrow indicate the relative convergence vector between the Pacific and Australian Plates from DeMets et al., (1994) and grey arrows show shortening rates at the Hikurangi Trough from Wallace et al. (2012). Abbreviations: NIDFB, North Island Dextral Fault Belt; TVZ, Taupo Volcanic Zone.

Geodetic measurements over the last 25 years have been used to determine New Zealand's contemporary surface strain field (Dimitrova et al., 2016; Haines &Wallace, 2020). The rotation of borehole-derived S_{Hmax} orientations along the HSM in the upper plate is remarkably consistent with the variation in coupling behavior on the HSM subduction interface (Figure 1b) and the along-strike rotation observed in the maximum contraction directions determined from geodetic measurements along the HSM forearc (Dimitrova et al., 2016; Haines & Wallace, 2020; Figure 6a). Maximum contraction directions determined from campaign GPS data reveal that the central HSM has a dominant E-W maximum contraction direction, whereas the southern HSM shows a NW-SE contraction direction (Figure 6a; Haines & Wallace, 2020), broadly compatible with the borehole-derived S_{Hmax} orientations reported here. The along-strike variations in maximum contraction directions from GPS are suggested to be related to along-strike changes in interseismic coupling on the HSM plate interface (Wallace et al., 2004; Dimitrova et al., 2016). In the northern and central HSM, the subduction interface is largely creeping and experiences shallow (<15 km), episodic slow slip events on the offshore. At the southern HSM the plate interface is strongly interseismically coupled to ~30 km depth, and is currently accumulating elastic strain in the surrounding crust that will eventually be relieved in future large earthquakes (Wallace, 2020; Figure 1b). The strong agreement between the geodetic maximum contraction directions and the observed stress field from the borehole observations indicate that S_{Hmax} orientations and their variability at HSM are strongly influenced by along-strike variations in elastic strain accumulation in

the overriding plate due to changes in interseismic coupling on the subduction interface.

In the central HSM (where the plate boundary is largely creeping) borehole-derived S_{Hmax} orientations and maximum contraction directions are reasonably consistent and sub-parallel to far-field relative Pacific-Australian plate motion. In contrast, at the southern HSM borehole-derived S_{Hmax} orientations and maximum contraction directions are roughly perpendicular to far-field relative Pacific-Australian plate motion, but are parallel to the convergence direction. This observation may be due to the fact that the subducting plate drags the forearc wedge in the direction of subduction and increases elastic compression strain and stress on the plate interface and within the forearc itself aligning elastic strain accumulation and S_{Hmax} stress orientations into that orientation. These S_{Hmax} orientation observations are at odds with those of Townend and Zoback (2006) showing that stress orientations in central Japan (from earthquake focal mechanisms) do not agree with maximum contraction directions associated with cyclical subduction zone locking. This difference in the conclusions between our study and Townend and Zoback (2006) may be related to the fact that we utilize shallow (<3 km) stress orientations, which may be more susceptible to temporal changes in elastic strain resulting from interseismic coupling rather than stress orientations from earthquake focal mechanisms sampling greater depths. This observation at the HSM may be reflecting longer-term accumulation of stress (related to long-term tectonic processes) independent of stage within the earthquake cycle.

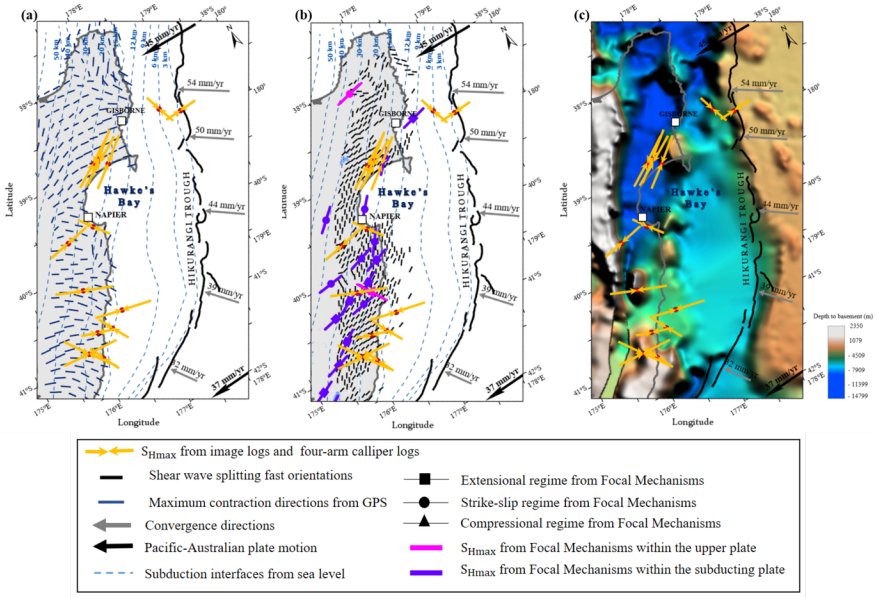

Figure 6. (a) Map of maximum contraction directions from GPS data (Haines & Wallace, 2020) and borehole-derived S_{Hmax} orientations (orange arrows) and IODP borehole image analysis from McNamara et al. (2021) (blue arrows). (b) Map of S_{Hmax} orientations and inferred faulting regime from focal plane mechanisms (0-60 km; square: extensional, circle: strike-slip, and triangle: compressional regime; Townend et al., 2012), seismic anisotropy measurements (0-40 km; black lines). Dashed blue lines show depth of subduction interface from sea level (Williams et al., 2013). (c) The map showing depth to basement map of North Island adapted from FROGTECH (2014). The clockwise rotation of S_{Hmax} orientation along the HSM strike follows the basement topography. Black arrows indicate the long-term motion of the Pacific relative to Australian Plate from DeMets et al., (1994) and grey arrows show shortening rates at the Hikurangi Trough from Wallace et al. (2012). Red dots show the borehole locations.

Although borehole-derived S_{Hmax} orientations at the HSM are broadly consistent with maximum contraction directions, S_{Hmax} orientations are not uniform within the forearc and in places deviate from the observed maximum contraction directions (Figure 6a). Some of these variabilities may be due to longer-term partitioning

of oblique relative motion and strain into margin-parallel, margin-perpendicular, and strike-slip components. Similar deviations from maximum contraction directions are observed within the Nankai subduction zone (Chang et al., 2010) and Costa Rica margin (Malinverno et. al, 2016). For example, borehole-derived S_{Hmax}orientations in the accretionary prism across the Nankai subduction zone are subparallel to the plate convergence vector between the Philippine Sea plate and Japan, perpendicular to the plate boundary, and for one borehole in the shelf edge is parallel to the plate boundary (Lin et al., 2010; Chang et al. 2010; Wu et al. 2012). The variations of stress among these sites and the deviation of borehole-derived S_{Hmax} orientations from the plate motion vectors derived from GPS data are suggested to be attributed to the strain partitioning into trench-parallel, right-lateral slip and thrust tectonics due to oblique plate convergence (Tobin et al. 2009; Lin et al. 2010). Alternatively, such stress variations have also been attributed to other factors such as thrusting and bending within individual geologic domains and local extension deformations derived by gravitation collapse of the prism in the forearc (Chang et al., 2010; Lin et al., 2016).

Townend et al. (2012) derived S_{Hmax} orientations from earthquake focal mechanisms using a Bayesian approach for earthquake data between 2004-2011 with $M_L > 3$. Their observations reveal that S_{Hmax} orientation changes from NE-SW in the central HSM to a more oblique S_{Hmax}orientation, sub-parallel to Pacific-Australia relative plate motion, in the southern HSM (Figure 6b). Only two focal mechanism solutions are located within the upper plate of the HSM or near the subduction interface; one strike-slip event with a NE-SW S_{Hmax}orientation (latitude 38°S; North of central HSM) at 7 km depth, and one compressional event with a WNW-ESE S_{Hmax} orientation (latitude 40.5°S; southern HSM) at 25 km depth (at the top of subducting plate near the subduction interface; Figure 6b). In the central HSM (where the plate boundary is largely creeping) borehole-derived NE-SW S_{Hmax} orientations and maximum contraction directions agree with the NE-SW S_{Hmax} orientations derived from focal mechanism inversions within the upper plate and subducting plate, implying that far-field plate boundary forces exerted at the HSM primarily control the present-day crustal stresses in the upper plate in this area. In contrast, the southern HSM shows stress field rotation with depth from borehole-derived WNW-ESE/NW-SE S_{Hmax}orientations (roughly margin-perpendicular) in the shallow crust of upper plate to NE-SW/ ENE-WSW focal mechanism-derived S_{Hmax} orientations within the subducting plate (Figure 6b). The NE-SW/ ENE-WSW S_{Hmax} orientations derived from focal mechanism inversions indicate a normal or strike-slip tectonic regime within the subducting plate of the southern HSM. There is one compressional event at ~25 km depth (near the subduction interface) where the borehole-derived S_{Hmax} orientation agrees with a focal mechanism-derived WNW-ESE S_{Hmax}orientation (latitude 40.5°S; Figure 6b). This implies that the overriding plate broadly is in a condition of horizontal compression parallel to convergence direction, potentially as deep as the plate interface (±10 km) (barring localized variations) and the tectonic regime becomes more strike-slip and normal within the subducting plate. The change in stress orientation with depth in the southern HSM is more compatible with a theoretically mechanically weak plate interface with low resolved shear stress and normal effective stress on the plate interface. The fact that the upper plate is in the state of horizontal compression parallel to plate convergence, on the other hand, implies that contemporary S_{Hmax} orientation is being driven by subduction of Hikurangi Plateau beneath North Island. Taking these observations into consideration, we propose that plate interface remains mechanically weak along the whole HSM and that a small increase of elastic compression strain and stress caused by the interseismically coupled southern HSM interface is sufficient to rotate S_{Hmax} orientation in the upper plate toward the subduction direction.

More recently, Illsley-Kemp et al. (2019) measured seismic anisotropy using shear wave splitting fast orientations from earthquake data in 2005–July 2018 with $M_L > 0$. Some studies consider fast orientations as a proxy for S_{Hmax}orientation if other significant crustal anisotropies are not present (e.g. fracturing, faulting, grain and crustal preferred orientations). The seismic anisotropy was derived from events [?]40 km deep and fast orientations were dominantly NE-SW (margin-parallel) for most of the HSM forearc, and more ENE-WSW in the northern and central HSM (Figure 6b). With the exception of some portions of the central HSM, the fast directions from shear-wave splitting studies do not agree well with the S_{Hmax} orientations we measure in the shallow boreholes. This could mean either (a) that the shear wave splitting fast directions are not controlled by contemporary S_{Hmax} orientation, or (b) that the fast directions are mainly controlled

by structural features such as faults and the stress state at greater depths, which may be different than the near-surface which our study samples. In fact, propagating waves sample the volume of crust above the hypocenter without taking the variation of anisotropic with depth into account.

Long-term tectonic deformation resulting from rapid clockwise rotation of the Hikurangi forearc (Wallace et al. 2004) may also possibly explain the along-strike variation in S_{Hmax} orientation. The clockwise rotation of forearc, which accommodates the margin-parallel component of oblique Pacific-Australian plate motion, results in significant tectonic transitions along the strike (Nicol et al., 2007; Wallace et al., 2004). Tectonic regime varies from back-arc rifting within the TVZ in the central part of North Island, strike-slip and normal faulting onshore of the northern and central HSM to transpression and reverse faulting at the southern HSM (Figure 5). The rotation of S_{Hmax} orientations from margin-parallel in the onshore central HSM to margin-perpendicular in the southern HSM likely reflects this transition in the tectonic regime, Such that the NE-SW S_{Hmax} orientation in the central HSM reflects margin-normal extension due to the transmission of slab rollback forces across the forearc and into the adjacent extensional back-arc rift (Wallace et al., 2012b). The clockwise rotation of the Hikurangi forearc may also explain why our observed contemporary S_{Hmax}orientation of NE-SW is not consistent with active large-scale NE-SW striking compressional faults in the central HSM. The imaged intervals of the central HSM boreholes are located within the hanging walls of active NE-SW striking compressional faults and within NE-SW oriented fault-bend fold axes identified from seismic reflection profiles (Western Energy New Zealand, 2001; Barnes et al., 2002). It is possible that the deformation and growing rate of these reverse faults within the central HSM have changed through time, allowing forces exerted by forearc rotation surpass the NW-SE compression stress on these active faults. In this case, the rotation of the forearc, which accommodates the margin-parallel component, induces a NE slip motion on these pre-existing faults. This also suggests that these reverse faults in the context of current stress field could be currently active as strike-/oblique-slip faults. Another possibility is that due to frequent earthquakes in this region, the S_{Hmax} orientation within the central HSM has changed from a potential NW-SE orientation perpendicular to the margin, compatible with the orientation of observed reverse faults and fold axes, to the contemporary NE-SW orientation subparallel to the margin. During the interseimic period, strain and stress accumulation along the reverse faults and subduction interface drives compression in the upper plate parallel to convergence direction. Following great earthquakes or frequent earthquakes, the margin-perpendicular component is reduced due to post-seismic stress release, allowing a strike-slip motion in direction of long-term oblique relative plate motion on these faults. This implies that the stress state associated with seismicity perturbations is quite long lasting (these boreholes are drilled over the course of 4 years) such that stress state require a long time to recover or the perturbations were significant enough to permanently reorient the stress. In this scenario, the intermediate principal stress (S_{hmin}) and minimum principal stress (S_v) would switch and principal stresses re-orient in response to forces exerted by long-term relative plate motion and fluctuations in the magnitude of stress parallel to plate convergence, modulated by the seismic cycles. Sacks et al. (2013) and Moore et al. (2013) used a similar concept to explain the contrast between S_{Hmax} orientations and normal fault strikes within Kumano Basin of the Nankai subduction zone.

Lateral variations in surface and basement topography may also play a role in the observed along-strike variation in upper plate borehole-derived S_{Hmax} orientations (Figure 6c). Basement structures such as faults, folds, and seamounts that are not covered by thick sediments can cause significant stress rotation at both regional and large scales by introducing geomechanical inhomogeneities and lateral discontinuities (Gale et al., 1984; Enever et al. 1999; Rajabi et al., 2016a). In fact, the presence of seamounts on the incoming plate have been suggested as a possible localized effect on stress field orientations and shear-wave splitting fast directions in the offshore northern HSM (McNamara et al., 2021; Zal et al., 2020). The SEEBASE model of New Zealand, a depth to basement map based on the integrated interpretation of gravity, magnetic, borehole, and seismic data (Figure 6c) clearly shows a significant change in sediment thickness overlying the basement rocks, and basement topography along the HSM margin (FROGTECH , 2014). The onshore northern and central HSM basement is located at depths ˜9-15 km and covered by thick Neogene sediments, whereas at the onshore and offshore southern HSM the Mesozoic greywacke basement is uplifted and located at relatively shallow depths (<5 km), and in some locations above sea level. Thin sediment

packages directly overlying mechanically strong basement rocks, may be more reflective of the tectonic stresses experienced by the basement. Hence, it is possible that the basement compressional structures striking NNE/NE-SSW/SW control the observed margin-perpendicular, NW-SE S_{Hmax} orientation within the shallow crust of the southern HSM.

In addition to large-scale stress variations, localized variations have been observed between and within individual boreholes which could be attributed to local active geological structures such as faults, surface topography, and variable mechanical properties. For instance a localized NW-SE S_{Hmax} orientation (144deg +- 11deg) is noted from four-arm caliper data in borehole Whakatu-1 (south of Napier; Figure 5), perpendicular to the dominant NE-SW S_{Hmax} orientation of the central HSM. The NW-SE S_{Hmax} orientation in Whakatu-1 is margin-perpendicular implying a localized compressional tectonic regime at this locale, which agrees well with observed onshore and offshore active, NNE-SSW striking, compressional faults in this region (Figure 5; Litchfield et al. (2014); Langridge et al, (2016)), such as the reverse fault responsible for growth of the Cape Kidnapper's anticline (Hull, 1987). Furthermore, Dimitrova et al. (2016) reported a possible locked patch in southern central HSM between shallow SSEs on the East Coast and deep Kaimanawa SSEs west of the East Coast (Figure 1b). Downdip changes in interseismic coupling behavior of the subduction interface and the accumulated strain associated with the locked patch could also be influencing the compressional tectonic regime in this region and borehole Whakatu-1.

6 Conclusions

This paper presents the first comprehensive analysis of contemporary S_{Hmax} orientations along the HSM, and discusses stress field orientation variability within the context of variable tectonics and slip behavior of this subduction margin. S_{Hmax}orientations in the central HSM are predominately NE-SW (sub-parallel to plate boundary), which rotates to a dominantly WNW-ESE S_{Hmax} orientation in the southern HSM (approximately perpendicular to the plate boundary). Our borehole-derived S_{Hmax} orientations agree with the maximum contraction strain directions from GPS measurements along the HSM suggesting that the observed stress orientations along the HSM are influenced by elastic strain accumulation due to interseismic coupling on the Hikurangi subduction interface. The long-term tectonic deformation arising from rapid rotation of the Hikurangi forearc, causing reverse faulting and strike-slip in the southern part of the margin and a combination of extension and strike-slip in the northern and central margin and the basement topography may also be at play in influencing the along-strike variations in observed stress orientations. In the southern HSM, borehole-derived S_{Hmax} orientations are inconsistent with S_{Hmax} orientations derived from focal mechanism solutions in the subducting plate, implying that the southern HSM interface is mechanically weak. Further interpretation of HSM stress state could be achieved by constraining stress magnitudes, which will be the focus of future studies.

Acknowledgments

This publication has emanated from research conducted with the financial support of Science Foundation Ireland (SFI) under Grant Number 17/RC-PhD/3481 and Geological survey of Ireland (GSI). The authors would like to thank the New Zealand Petroleum and Minerals group (NZPM) within the Ministry for Business, Innovation and Employment (MBIE) for providing access to borehole data and supporting materials for this study. We also thank Schlumberger for providing academic licenses for Techlog 2018.1 to University College Dublin and University of Liverpool. We thank to Esri for providing the academic license of ArcGIS Pro. For the purpose of Open Access, the author has applied a CC BY public copyright license to any Author Accepted Manuscript version arising from this submission.

Data Availability Statement

This research used data provided by the New Zealand Petroleum and Minerals group (NZPM) within the Ministry for Business, Innovation and Employment (MBIE). The borehole image logs and oriented four-arm caliper data used in this paper can accessed through MBIE 's database. All additional data used in this article was collected from published sources referenced in the text. In Supporting Information, data set 1 contains all borehole breakouts presented in this study.

References

Aadnoy, B. S., & Bell, J. S. (1998), Classification of drill-induce fractures and their relationship to in-situ stress directions. *The Log Analyst*, *39* (06), 27–42. Bailleul, J., Chanier, F., Ferriere, J., Robin, C., Nicol, A., Mahieux, G., et al. (2013), Neogene evolution of lower trench-slope basins and wedge development in the central hikurangi subduction margin, new zealand. *Tectonophysics*, *591*, 152–174.*https://doi.org/10.1016/j.tecto.2013.01.003*Barnes, P. M., Lamarche, G., Bialas, J., Henrys, S., Pecher, I., Netzeband, G. L., et al. (2010), Tectonic and geological framework for gas hydrates and cold seeps on the Hikurangi Subduction Margin, New Zealand. Marine Geology, 272(1–4), 26–48.*https://doi.org/10.1016/j.margeo.2009.03.012*Barnes, P. M., Lpinay, M. De, Collot, J. Y., Delteil, J., & Audru, J.-C. (1998), Strain partitioning in the transition area between oblique subduction and continental collision, Hikurangi margin.*Tectonics*, *17*(4), 534–557. Barnes, P. M., Nicol, A., & Harrison, T. (2002), Late Cenozoic evolution and earthquake potential of an active listric thrust complex above the Hikurangi subduction zone, New Zealand. *Bulletin of the Geological Society of America*, *114*(11), 1379–1405.*https://doi.org/10.1130/0016-7606(2002)114<1379:LCEAEP>2.0.CO;2*Barton, C. A., Hickman, S., Morin, R., Zoback, M. D., & Benoit, D. (1998), Reservoir-scale fracture permeability in the Dixie Valley, Nevada, geothermal field. SPE/ISRM Rock Mechanics in Petroleum Engineering, Trondheim, Norway, July 1998, 47371, 315–322. Barton, C., & Moos, D. (2010), Geomechanical wellbore imaging: Key to managing the asset life cycle, in M. Po"ppelreiter, C. Garcı´a- Carballido, and M. Kraaijveld, eds., Dipmeter and borehole image log technology: *American Association of Petroleum Geologists Memoir*,*92*, 1–32.*https://doi.org/10.1306/13181279M922689*Beanland, S., & Haines, J. (1998), The kinematics of active deformation in the North Island, New Zealand, determined from geological strain rates. *New Zealand Journal of Geology and Geophysics*,*41*(4), 311–323.*https://doi.org/10.1080/00288306.1998.9514813*Bell, J. S. (2003), Practical methods for estimating in situ stresses for borehole stability applications in sedimentary basins. *Journal of Petroleum Science and Engineering*, *38*(3–4), 111–119.*https://doi.org/10.1016/S0920-4105(03)00025-1*Bell, J. S., & Gough, D. I. (1979), Northeast-southwest compressive stress in Alberta evidence from oil wells. *Earth and Planetary Science Letters*, *45*(2), 475–482.*https://doi.org/10.1016/0012-821X(79)90146-8*Berryman, K., Marden, M., Palmer, A., & Litchfield, N. (2009), Holocene rupture of the Repongaere fault, Gisborne : Implications for Raukumara Peninsula deformation and impact on the Waipaoa Sedimentary System Holocene rupture of the Repongaere Fault, Gisborne : and impact on the Waipaoa Sedimentary System. *New Zealand Journal of Geology and Geophysics*, *52*(4), 335–347.*https://doi.org/10.1080/00288306.2009.9518462*Brodsky, E. E., Saffer, D., Fulton, P., Chester, F., Conin, M., Huffman, K., et al. (2017), The postearthquake stress state on the Tohoku megathrust as constrained by reanalysis of the JFAST breakout data.*Geophysical Research Letters*, *44*, 8294–8302.*https://doi.org/10.1002/2017GL074027*Brudy, M., & Zoback, M. D. (1999), Drilling-induced tensile wall-fractures: Implications for determination of in-situ stress orientation and magnitude. *International Journal of Rock Mechanics and Mining Sciences*, *36*, 191–215.*https://doi.org/10.1016/S0148-9062(98)00182-X*Byrne, T. B., Lin, W., Tsutsumi, A., Yamamoto, Y., Lewis, J. C., Kanagawa, K., et al. (2009), Anelastic strain recovery reveals extension across SW Japan subduction zone Anelastic strain recovery reveals extension across SW Japan subduction zone. *Geophysical Research Letters*, *36*(L23310).*https://doi.org/10.1029/2009GL040749*Chang, C., McNeill, L. C., Moore, J. C., Lin, W., Conin, M., & Yamada, Y. (2010), In situ stress state in the Nankai accretionary wedge estimated from borehole wall failures. *Geochemistry, Geophysics, Geosystems*, *11*(12), 1–17.*https://doi.org/10.1029/2010GC003261*Chanier, F., Ferriere, J., & Angelier, J. (1999), Extensional deformation across an active margin, relations with subsidence, uplift, and rotations: The Hikurangi subduction, New Zealand. *Tectonics*,*18*(5), 862–876. Davatzes, N. C., & Hickman, S. H. (2010), Stress, fracture, and fluid-flow analysis using acoustic and electrical image logs in hot fractured granites of the Coso geothermal field, California, U.S.A. In M. Po"ppelreiter, C. Garcı´a-Carballido, and M. Kraaijveld, eds., Dipmeter and borehole image log technology (259–293).*https://doi.org/10.1306/13181288M923134*Davy, B. W. (1992), The influence of subducting plate buoyancy on subduction of the Hikurangi-Chatham Plateau beneath the North Island, New Zealand. *Geology and Geophysics of Continental Margins*. Davy, B., Hoernle, K., & Werner, R. (2008), Hikurangi Plateau: crustal structure, rifted formation, and Gondwana subduction history.*Geochemistry, Geophysics, Geosystems*, *9*(7). https://doi.org/10.1029/2007GC001855 DeMets, C.,

Gordon, R. G., Argus, D. F. & Stein, S. (1994), Effect of recent revisions to the geomagnetic reversal time scale on estimates of current plate motions. *Geophysical Research Letters*, *21*, 2191–2194. Dimitrova, L. L., Wallace, L. M., Haines, A. J., & Williams, C. A. (2016), High-resolution view of active tectonic deformation along the Hikurangi subduction margin and the Taupo Volcanic Zone, New Zealand.*New Zealand Journal of Geology and Geophysics*, *59*(1), 43–57.*https://doi.org/10.1080/00288306.2015.1127823*Enever, J. R., Gale, W. & Fabjanczvk, M. (1999), A study of the variability of the horizontal stress field in a sedimentary basin.*9th International Society for Rock Mechanics Congress*, Paris, France, 1257-1260. Fellgett, M. W., Kingdon, A., Waters, C. N., Field, L., Shreeve, J., Dobbs, M., & Ougier-simonin, A. (2019), Lithological constraints on borehole wall failure ; a study on the Pennine coal measures of the United Kingdom. *Frontiers in Earth Science*, *7*(163).*https://doi.org/10.3389/feart.2019.00163*FROGTECH. (2014), New Zealand Basement Composition and Heat Flow GIS Project. Report prepared for the Government of New Zealand, Department of Petroleum and Minerals. Gale, W. J., Enever, J. R., Blackwood, R. L. & McKay, J. (1984), An investigation of the effect of a fault /monocline structure on the in-situ stress field and mining conditions at Nattai Bulli Colliery NSW, Australia. CSIRO Australia, Division of Geomechanics. Geomechanics of Coal Mining Report No. 48. Ghisetti, F. C., Barnes, P. M., Ellis, S., Plaza-Faverola, A. A., & Barker, D. H. N. (2016), The last 2 Myr of accretionary wedge construction in the central Hikurangi margin (North Island, New Zealand): Insights from structural modeling. *Geochemistry, Geophysics, Geosystems*, *17*(11), 4517–4533. *https://doi.org/10.1002/2016GC006341*Griffin, A. G. (2019), Subsurface S_{HMAX} determined from a borehole image log, onshore southern East Coast Basin, New Zealand.*New Zealand Journal of Geology and Geophysics*, *62*(2), 273–290. https://doi.org/10.1080/00288306.2019.1570946 Griffin, A. G., Bland, K. J., Morgans, H. E. G., Strogen, D. P. (2021), A multifaceted study of the offshore Titihaoa-1 drillhole and a Neogene accretionary slope basin , Hikurangi subduction margin. *New Zealand Journal of Geology and Geophysics*. https://doi.org/10.1080/00288306.2021.1932527 Haines, A. J., & Wallace, L. M. (2020), New Zealand-wide geodetic strain rates using a physics-based approach. *Geophysical Research Letters*, *47*(1).*https://doi.org/10.1029/2019GL084606*Hardebeck, J. L. (2004), Stress triggering and earthquake probability estimates. *Journal of Geophysical Research*, *109*(B04310).*http://dx.doi.org/10.1029/2003JB002437*Hardebeck, J. L., & Okada, T. (2018), Temporal stress changes caused by earthquakes: a review. *Journal of Geophysical Research : Solid Earth*, *123*, 1350–1365.*https://doi.org/10.1002/2017JB014617*Heidbach, O., Barth, A., Muller, B., Reinecker, J., Stephansson, O., Tingay, M., & Zang, A. (2016), WSM quality ranking scheme, database description and analysis guidelines for stress indicator. World Stress Map Technical Report 16-01. GFZ German Research Centre for Geosciences. http://doi.org/10.2312/wsm.2016.001 Heidbach, O., Rajabi, M., Cui, X., Fuchs, K., Muller, B., Reinecker, J., et al. (2018), The world stress map database release 2016: crustal stress pattern across scales. *Tectonophysics*, *744*, 484–98. *https ://doi.org/10.1016/j.tecto .2018.07.007*Huffman, K. A., & Saffer, D. M. (2016), In situ stress magnitudes at the toe of the Nankai Trough accretionary prism, offshore Shikoku Island, Japan. *Journal of Geophysical Research : Solid Earth*,*121*, 1202–1217. https://doi.org/10.1002/2015JB012415 Hull, A. (1987), A late holocene marine terrace on the kidnappers coast, north island , new zealand : some implications for shore platform development processes and uplift mechanism. *Quaternary Research*,*28*(2), 183–195. Illsley-Kemp, F., Savage, M. K., Wilson, C. J. N., & Bannister, S. (2019), Mapping stress and structure from subducting slab to magmatic rift: crustal seismic anisotropy of the North Island, New Zealand.*Geochemistry, Geophysics, Geosystems*, *20.https://doi.org/10.1029/2019gc008529*Jaeger, J., Cook, N., & Zimmerman, R. (2007), Fundamentals of rock mechanics. *Wiley-Blackwell.https://doi.org/10.1017/CBO9780511735349*King, R. C., Tingay, M. R. P., Hillis, R. R., Morley, C. K., & Clark, J. (2010), Present-day stress orientations and tectonic provinces of the NW Borneo collisional margin. *Journal of Geophysical Research: Solid Earth*, *115*(10).*https://doi.org/10.1029/2009JB006997*Kingdon, A., Fellgett, M. W., & Williams, J. D. O. (2016), Use of borehole imaging to improve understanding of the in-situ stress orientation of Central and Northern England and its implications for unconventional hydrocarbon resources. *Marine and Petroleum Geology*, *73*, 1–20.*https://doi.org/10.1016/j.marpetgeo.2016.02.012*Kulander, B. R., Dean, S. L., & Ward Jr., B. J. (1990), Fractured core analysis: Interpretation, logging, and use of natural and induced fractures in core. American Association of Petroleum Geologists, 8, Tulsa, Okla-

homa.Laird, M. G., & Bradshaw, J. D. (2004), The break-up of a long-term relationship : the Cretaceous separation of New Zealand from Gondwana. *Gondwana Research*, *7*(I), 273–286. Langridge, R. M., Ries, W. F., Litchfield, N. J., Villamor, P., Van Dissen, R. J., Barrell, D. J. A., et al. (2016), The New Zealand active faults database. *New Zealand Journal of Geology and Geophysics*,*59* (1), 86–96.*https://doi.org/10.1080/00288306.2015.1112818*Lawrence, M. J. F. (2018), Structural and Sedimentological Interpretation of Well Data from the Wairoa Area, North Island, New Zealand. GNS Science Report 2018/28, 1–76.*https://doi.org/10.21420/G23W81*Li, Y., & Schmitt, D. R. (1998), Drilling-induced core fractures and in situ stress. Journal of Geophysical Research, 103(B3), 5225–5239. Lin, W., Byrne, T. B., Kinoshita, M., Mcneill, L. C., Chang, C., Lewis, J. C., Yamamoto, Y., et al. (2016), Distribution of stress state in the Nankai subduction zone, southwest Japan and a comparison with Japan Trench. *Tectonophysics*, *692*, 120–130.*https://doi.org/10.1016/j.tecto.2015.05.008*Lin, W., Conin, M., Moore, J. C., Chester, F. M., Nakamura, Y., Mori, J. J., Anderson, L., et al. (2013), Stress State in the Largest Displacement Area of the 2011 Tohoku-Oki Earthquake. *Science*,*339*(687).*https://doi.org/10.1126/science.1229379*Lin, W., Doan, M. L., Moore, J. C., McNeill, L., Byrne, T. B., Ito, T., et al. (2010), Present-day principal horizontal stress orientations in the Kumano forearc basin of the southwest Japan subduction zone determined from IODP NanTroSEIZE drilling Site C0009. *Geophysical Research Letters*, *37*(13), 1–6.*https://doi.org/10.1029/2010GL043158*Lin, W., Yeh, E., Ito, H., Hung, J., Hirono, T., Soh, W., et al. (2007), Current stress state and principal stress rotations in the vicinity of the Chelungpu fault induced by the 1999 Chi-Chi , Taiwan , earthquake.*Geophysical Research Letters*, *34*(L16307). https://doi.org/10.1029/2007GL030515 Litchfield, N. J., Van Dissen, R., Sutherland, R., Barnes, P. M., Cox, S. C., Norris, R., et al. (2014), A model of active faulting in New Zealand. *New Zealand Journal of Geology and Geophysics*,*57*(1), 32–56.*https://doi.org/10.1080/00288306.2013.854256*Little, T. A., & Roberts, A. P. (1997), Distribution and mechanism of Neogene to present-day vertical axis rotations , Pacific-Australian plate boundary. *Journal of Geophysical Research*, *102*, 20447–20468. Ma, K. F., Chan, C. H., & Stein, R. S. (2005), Response of seismicity to Coulomb stress triggers and shadows of the 1999 Mw = 7.6 Chi-Chi, Taiwan, earthquake. *Journal of Geophysical Research*, *110*, B05S19.*http://dx.doi.org/10.1029/2004JB003389*Magee, M. E., & Zoback , M. D. (1993), Evidence for a weak interplate thrust fault along the northern Japan subduction zone and implications for the mechanics of thrust faulting and fluid expulsion,*Geology*, *21*, 809–812. Malinverno, A., Saito, S., & Vannucchi, P. (2016), Horizontal principal stress orientation in the Costa Rica Seismogenesis Project (CRISP) transect from borehole breakouts. *Geochemistry, Geophysics, Geosystems*, *17*(1), 65–77.*https://doi.org/10.1002/2015GC006092*McNamara, D. D., Behboudi, E., Wallace, L., Saffer, D. M., Cook, A. E., Fagereng, A., et al (2021), Variable in-situ stress orientations across the northern Hikurangi Subduction Margin. *Geophysical Research Letters.https://doi.org/10.1029/2020GL091707*Mochizuki, K., Sutherland, R., Henrys, S., Bassett, D., Van Avendonk, H., Arai, R., et al. (2019), Recycling of depleted continental mantle by subduction and plumes at the Hikurangi Plateau large igneous province, southwestern Pacific Ocean. *Geology*, *47*(8), 795–798.*https://doi.org/10.1130/G46250.1*Moore, G. F., Boston, B. B., Sacks, A. F., & Saffer, D. M. (2013), Analysis of normal fault populations in the Kumano Forearc Basin , Nankai Trough , Japan : 1 . Multiple orientations and generations of faults from 3-D coherency mapping. *Geochemistry, Geophysics, Geosystems*, *114*, 1989–2002. https://doi.org/10.1002/ggge.20119 Mountjoy, J. J., & Barnes, P. M. (2011), Active upper plate thrust faulting in regions of low plate interface coupling, repeated slow slip events, and coastal uplift: Example from the Hikurangi Margin, New Zealand. *Geochemistry*, *12*(1), Q01005. https://doi. org/10.1029/2010gc003326 Nicol, A., & Beavan, J. (2003), Shortening of an overriding plate and its implications for slip on a subduction thrust, central Hikurangi Margin, *New Zealand. Tectonics*, *22*(6),*https://doi.org/10.1029/2003TC001521*Nicol, A., Mazengarb, C., Chanier, F., Rait, G., Uruski, C., & Wallace, L. (2007), Tectonic evolution of the active Hikurangi subduction margin, New Zealand, since the Oligocene. *Tectonics*, *26*(4), 1–24.*https://doi.org/10.1029/2006TC002090*Nicol, A., VanDissen, R., Vella, P., Alloway, B., & Melhuish, A. (2002), Growth of contractional structures during the last 10 m.y. at the southern end of the emergent Hikurangi forearc basin, New Zealand.*New Zealand Journal of Geology and Geophysics*, *45*(3), 365–385.*https://doi.org/10.1080/00288306.2002.9514979*Pedley, K. L., Barnes, P. M., Pettinga, J. R., & Lewis, K. B. (2010), Seafloor structural geomorphic evolution of the accretionary frontal wedge in response to seamount subduction, Poverty Indentation, New Zealand. *Marine Geology*, *270*(1–4),

119–138. https://doi.org/10.1016/j. margeo.2009.11.006 Peška, P., & Zoback, M. D. (1995), Compressive and tensile failure of inclined well bores and determination of in situ stress and rock strength. *Journal of Geophysical Research*, *100*(B7), 12791–12811. Pettinga, J. R. (2004), Three - stage massive gravitational collapse of the emergent imbricate frontal wedge , Hikurangi Subduction Zone , New Zealand. *New Zealand Journal of Geology and Geophysics*,*47*(3), 399–414.*https://doi.org/10.1080/00288306.2004.9515066*Rajabi, M., Tingay, M., & Heidbach, O. (2016a), The present-day stress field of New South Wales, Australia. *Australian Journal of Earth Sciences*, *63*(1), 1–21.*https://doi.org/10.1080/08120099.2016.1135821*Rajabi, M., Tingay, M., & Heidbach, O. (2016b), The present-day state of tectonic stress in the Darling Basin, Australia: Implications for exploration and production. *Marine and Petroleum Geology*,*77*, 776–790.*https://doi.org/10.1016/j.marpetgeo.2016.07.021*Reinecker, J., Tingay, M. R. P., & Müller, B. B. (2003), Borehole breakout analysis from four-arm caliper logs, World Stress Map Project Guidelines World Stress Map Project-Guidelines Four-arm Caliper Logs, 1-5. Sacks, A., Saffer, D. M., & Fisher, D. (2013), Analysis of normal fault populations in the Kumano forearc basin, Nankai Trough, Japan: 2. Principal axes of stress and strain from inversion of fault orientations. *Geochemistry, Geophysics, Geosystems*, *14*(6), 1973–1988.*https://doi.org/10.1002/ggge.20118*Schellart, W. P., & Rawlinson, N. (2013), Global correlations between maximum magnitudes of subduction zone interface thrust earthquakes and physical parameters of subduction zones. *Physics of the Earth and Planetary Interiors*, *225*, 41-67.*https://doi.org/10.1016/j.pepi.2013.10.001*Seeber, L., & Armbruster, J.G. (2000), Earthquakes as beacons of stress change. *Nature*, *407*, 69–72. Stein, R. S. (1999), The role of stress transfer in earthquake occurrence. *Nature*, *402*, 605–609. Tingay, M., Reinecker, J., & Müller, B. (2008), Borehole breakout and drilling-induced fracture analysis from image logs. World Stress Map Project-Guidelines: Image Logs, 1-8. Tobin, H., Kinoshita, M., Ashi, J., Lallemant, S., Kimura, G., Screaton, E., et al. (2009), NanTroSEIZE Stage 1 expeditions : introduction and synthesis of key results. In *Proceedings of the Integrated Ocean Drilling Program: 314/315/31.* https://doi.org/10.2204/iodp.proc.314315316.101.2009 Townend, J., & Zoback, M. D. (2006), Stress, strain, and mountain building in central Japan. *Journal of Geophysical Research: Solid Earth*, *111*(3), 1–11.*https://doi.org/10.1029/2005JB003759*Townend, J., Sherburn, S., Arnold, R., Boese, C., & Woods, L. (2012), Three-dimensional variations in present-day tectonic stress along the Australia-Pacific plate boundary in New Zealand. *Earth and Planetary Science Letters*, 353–354, 47–59.*https://doi.org/10.1016/j.epsl.2012.08.003*Vavryčuk V. (2015), Earthquake Mechanisms and Stress Field. In:*Beer M., Kougioumtzoglou I., Patelli E., Au IK. (Eds) Encyclopedia of Earthquake Engineering.* Springer, Berlin, Heidelberg.*https://doi.org/10.1007/978-3-642-36197-5_295-1*Walcott, R. I. (1987), Geodetic strain and the deformation history of the North Island of New Zealand during the late Cainozoic. Philosophical Transactions of the Royal Society of London. Series A,*Mathematical and Physical Sciences*, *321*, 163-181. Wallace, L. M. (2020), Slow Slip Events in New Zealand. *Annual Review of Earth and Planetary Sciences*, 1–29. Wallace, L. M., & Beavan, J. (2010), Diverse slow slip behavior at the Hikurangi subduction margin, New Zealand. *Journal of Geophysical Research: Solid Earth*, *115*(12), 1–20.*https://doi.org/10.1029/2010JB007717*Wallace, L. M., & Eberhart-Phillips, D. (2013), Newly observed, deep slow slip events at the central Hikurangi margin, New Zealand: Implications for downdip variability of slow slip and tremor, and relationship to seismic structure. *Geophysical Research Letters*,*40*(20), 5393–5398.*https://doi.org/10.1002/2013gl057682*Wallace, L. M., Beavan, J., Bannister, S., & Williams, C. (2012a), Simultaneous long-term and short-term slow slip events at the Hikurangi subduction margin , New Zealand : Implications for processes that control slow slip event occurrence, duration, and migration.*Journal of Geophysical Research*, *117*(B11402). https://doi.org/10.1029/2012JB009489 Wallace, L. M., Beavan, J., McCaffrey, R., & Darby, D. (2004), Subduction zone coupling and tectonic block rotations in the North Island, *New Zealand. Journal of Geophysical Research: Solid Earth*, *109*(12), 1–21.*https://doi.org/10.1029/2004JB003241*Wallace, L. M., Fagereng, Å., & Ellis, S. (2012b), Upper plate tectonic stress state may infl uence interseismic coupling on subduction megathrusts. *Geology*, *40*(10), 895–898.*https://doi.org/10.1130/G33373.1*Wenning, Q. C., Berthet, T., Ask, M., Zappone, A., Rosberg, J. E., & Almqvist, B. S. G. (2017), Image log analysis of in situ stress orientation, breakout growth, and natural geologic structures to 2.5 km depth in central Scandinavian Caledonides: Results from the COSC-1 borehole. *Journal of Geophysical Research: Solid Earth*,*122*(5), 3999–4019.*https://doi.org/10.1002/2016JB013776*Western

Energy New Zealand. (2001), Well Completion Report Kauhauroa-4B, Ministry of Economic Development New Zealand, Unpublished Open file Petroleum Report 2610. Williams, C. A., Eberhart-Phillips, D., Bannister, S., Barker, D. H. N., Henrys, S., Reyners, M., & Sutherland, R. (2013), Revised interface geometry for the hikurangi subduction zone, *New Zealand. Seismological Research Letters*, *84*(6), 1066–1073.*https://doi.org/10.1785/0220130035*Wu, H., Kinoshita, M., & Sanada, Y. (2012), Stress state estimation by geophysical logs in NanTroSEIZE Expedition 319-Site C0009, Kumano Basin , southwest Japan. *Geophysical Research Letters*,*39*(L18303).*https://doi.org/10.1029/2012GL053086*Zal, H. J., Jacobs, K., Savage, M. K., Yarce, J., Mroczek, S., Graham, K., et al. (2020), Temporal and spatial variations in seismic anisotropy and VP/VS ratios in a region of slow slip. *Earth and Planetary Science Letters*, *532*, 115970.*https://doi.org/10.1016/j.epsl.2019.115970*Zoback, M. D. (2007), Reservoir Geomechanics. Cambridge University Press. Zoback, M. D., Zoback, M. L., Eaton, J. P. , Mount, V. S. & Suppe, J. (1987), New evidence on the state of stress of the San Andreas Fault,*Science, 238*, 1105–1111. https://doi:10.1126/science.238.4830.1105.

Hosted file

`suppinfo_spatial variation of in-situ stress orientation along the hikurangi subduction margin insights` available at https://authorea.com/users/531433/articles/597644-spatial-variation-of-in-situ-stress-orientation-along-the-hikurangi-subduction-margin-insights-from-borehole-image-logging

E. Behboudi[1,2], D.D. McNamara[3], I. Lokmer[1,2], L. Wallace[4,5], and D. Saffer [5]

[1] Irish Centre for Applied Geosciences (iCRAG), University College Dublin, Republic of Ireland.

[2] School of Earth Sciences, University College Dublin, Republic of Ireland.

[3] Department of Earth, Ocean and Ecological Sciences, University of Liverpool, UK.

[4] GNS Science, New Zealand.

[5] University of Texas Institute for Geophysics, USA.

Corresponding author: Effat Behboudi (`effat.behboudi@ucdconnect.ie`)

Key Points:

- Maximum horizontal stress orientation varies along strike in the Hikurangi Subduction Margin upper plate
- Stress orientations reflect contemporary elastic strain accumulation processes related to subduction megathrust locking
- Stress orientations in the southern HSM are oblique to focal-mechanism stress suggesting the subduction interface is mechanically weak

Abstract

Knowledge of the contemporary in-situ stress orientations in the Earth's crust can improve our understanding of active crustal deformation, geodynamic processes, and seismicity in tectonically active regions such as the Hikurangi Subduction Margin (HSM), New Zealand. The HSM subduction interface is characterized by varying slip behavior along strike, which may be a manifestation of variation in the stress state and the mechanical strength of faults and their hanging walls, or, alternatively, these variations in seismic behavior may generate variation in the stress state in space and time. In this study, we analyze borehole image and oriented four-arm caliper logs acquired from thirteen boreholes along the HSM to present the first comprehensive stress orientation dataset within the HSM upper plate. Our results reveal a NE-SW S_{Hmax} orientation (parallel to the Hikurangi margin) within the central HSM (Hawke's Bay region) which rotates to a WNW- ESE S_{Hmax} orientation (roughly perpendicular to the Hikurangi margin) in the southern HSM. This rotation of S_{Hmax} orientation spatially correlates with along-strike variations in subduction interface slip behavior, characterized by creep and/or shallow episodic slip events in the central HSM and interseismic locking in the southern HSM. Observed borehole S_{Hmax} orientations are largely parallel to maximum contraction directions derived from geodetic surface deformation measurements, suggesting that modern stress orientations may reflect contemporary elastic strain accumulation processes related to subduction megathrust locking.

Plain Language Summery

Movement along faults at tectonic plate boundaries can cause changes in the orientations of the forces, known as stress, that make them move. Such changes may help us explain how deformation at the surface occurs when these faults move, the way fluid moves along these faults, and why different types of earthquakes occur on these faults. The Hikurangi Subduction Margin, New Zealand's largest and most hazardous plate boundary fault, shows a variety of deformation and earthquake types that occur in the over-riding plate which may be linked to stress orientation. In this study, we found that variability in the stress orientations within the upper plate of Hikurangi Subduction Margin matches areas where we see different earthquake types occurring, and observed patterns of surface deformation. We suggest that stress orientations reflect the accumulation and release of strain caused by subduction at the HSM.

1 Introduction

In-situ stress measurements can provide important insights into stress states at global and localized scales, the geomechanical state of earthquake-hosting faults, shear traction on faults, and processes of stress accumulation and release on plate boundary faults. Such measurements also assist with understanding how crustal stresses relate to strain observed geodetically and geologically (e.g., Zoback et al., 1987; Magee & Zoback, 1993; Townend & Zoback, 2006; Byrne et al., 2009; Chang et al., 2010; Lin et al., 2013, 2016; Brodsky et al., 2017). Earthquake occurrence and many earthquake rupture characteristics are partly dependent on the shear to normal stress ratio, which is a function of the relative magnitude of in-situ principal stresses, the orientation of the fault plane with respect to the orientation of the principal stress orientations, pore pressure, and fault plane friction coefficients (Jaeger et al., 2007; Schellart & Rawlinson, 2013; Vavryčuk, 2015). Additionally, earthquakes can redistribute stress and change both shear and normal stress on adjacent fault planes and surrounding rocks either statically (a shift in the stress state from before to after the earthquake) or dynamically (oscillating stress changes that occur with the passage of seismic waves) (Stein, 1999; Seeber & Armbruster, 2000; Hardebeck, 2004; Ma et al., 2005; Lin et al., 2007, 2016; Hardebeck & Okada, 2018).

The Hikurangi Subduction Margin (HSM), on the east coast of the North Island of New Zealand (Figure 1a), experiences strong along-strike variations in megathrust slip behaviour, ranging from deep interseismic locking (and stress accumulation) beneath the southern North Island, to episodic slow slip events (SSEs) and creep at the northern and central HSM (Figure 1b). Creep and shallow (<15 km depth) SSEs lasting for 2-3 weeks recur every 18-24 months offshore of the northern and central HSM (Wallace & Beavan 2010; Wallace, 2020; Figure 1b). Deep (>25 km), long-term (>1 year) slow slip events occur approximately every ~5 years at the southern HSM (Wallace & Beavan 2010), just down-dip of a portion of the plate interface that is strongly locked and accumulating stress likely to be released in a future great earthquake (Mw > 8.0). Despite the recognized importance of in-situ stress states along active subduction zones in understanding strain accumulation and release, few studies have

been undertaken to directly estimate stress magnitudes in these settings (Chang et al., 2010; Huffman & Saffer, 2016; Lin et al., 2010, 2013, 2016; Malinverno et al., 2016; Brodsky et al., 2017; McNamara et al., 2021).

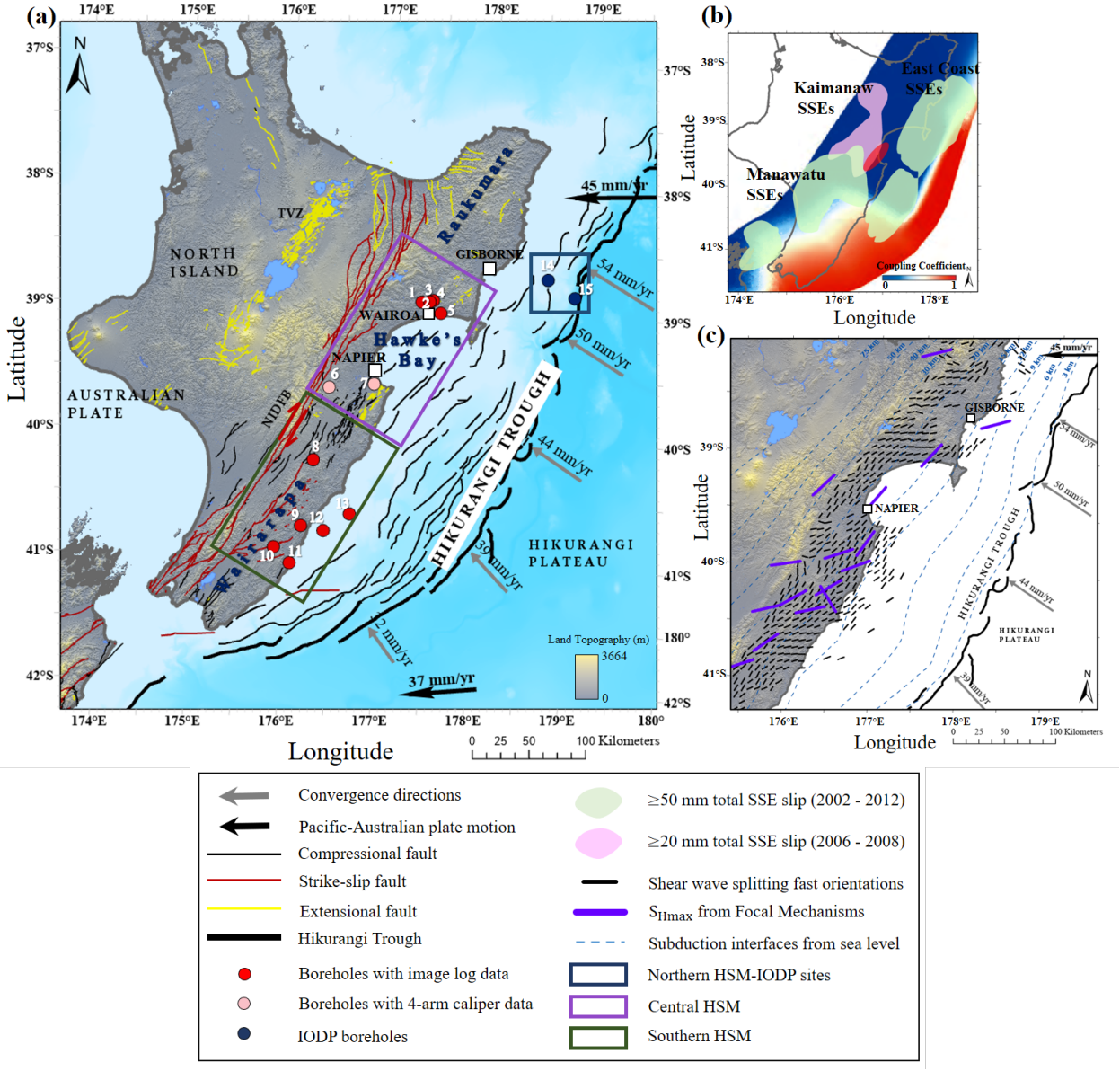

Figure 1. (a) Tectonic setting of East Coast of North Island, New Zealand. Fault traces from Barnes et al., (2010), Langridge et al, (2016), Mountjoy and Barnes (2011), and Pedley et al., (2010). Black arrows indicate the long-term motion of the Pacific relative to Australian Plate from DeMets et al., (1994)

and grey arrows show shortening rates at the Hikurangi Trough from Wallace et al. (2012). (b) Interseismic coupling based on campaign GPS velocities (1995–2008), shown in terms of coupling coefficient (Wallace et al. 2012a). Green and pink shaded regions represent the cumulative slow slips in 2002 and 2012 (Wallace et al., 2012a) and SSEs beneath the Kaimanawa ranges in 2006 and 2008 (Wallace & Eberhart-Phillips, 2013; Wallace, 2020). Area of possible locked patch between the East Coast and Kaimanaw SSEs is shaded in red. (c) Map showing S_{Hmax} orientations from focal mechanisms (Townend et al., 2012) and shear wave splitting fast orientations (Illsley-Kemp et al., 2019). Boreholes are numbered 1: Makareo-1, 2: Kauhauroa-2, 3: Waitahora-1, 4: Kauhauroa-5, 5: Tuhara-1A, 6: Kereru -1, 7: Whakatu-1, 8: Ngapaeruru-1, 9: Te Mai-2, 10: Rauni-2, 11: Orui-1A, 12: Titihaoa-1, 13: Tawatawa-1, 14: U1519A, and 15: U1518B. Abbreviations: NIDFB, North Island Dextral Fault Belt; TVZ, Taupo Volcanic Zone.

To date, several studies have been carried out to determine the contemporary in-situ stress patterns along the East Coast of the HSM. Analysis of earthquake focal mechanism solutions reveal that S_{Hmax} orientations in the crust (60 km depth) change from NE-SW (roughly margin-parallel; Figure 1c) in the northern and central Hikurangi margin to a more margin-oblique, ENE-WSW orientation, sub-parallel to Pacific/Australia relative plate motion, further south (Figure 1c). These measurements are largely from earthquakes within the subducting slab most located at depths >25 km depth (Townend et al., 2012). In contrast, the seismic anisotropy fast orientations determined from shear wave splitting methods that sample the upper ~40 km (Figure 1c) suggest a dominant S_{Hmax} orientation of NE-SW for most of the HSM forearc (generally margin-parallel), while the northern HSM forearc displays variable fast orientations, with a more dominant ENE-WSW inferred S_{Hmax} orientation (Illsley-Kemp et al., 2019). Shallow (<3km) S_{Hmax} orientations have been determined from limited analysis of borehole image logs from boreholes drilled onshore and offshore HSM (Heidbach et al., 2018; Lawrence, 2018; Griffin, 2019; Griffin et al., 2021; McNamara et al., 2021). Analysis of borehole image data from four onshore boreholes show NE-SW to ENE-WSW S_{Hmax} orientations in the central HSM (Heidbach et al., 2018; Lawrence, 2018;), and an E-W to NW-SE SHmax orientation is determined from two borehole image logs in the southern HSM (Heidbach et al., 2018; Griffin, 2019; Griffin et. al, 2021). Boreholes offshore the northern HSM drilled as part of the International Ocean Discovery Program (IODP) Expeditions 372 and 375 show an E-W S_{Hmax} orientation close to the Hikurangi trench, and a NW-SE S_{Hmax} orientation in the offshore forearc (McNamara et al., 2021), indicating strong variations in stress orientations across the forearc.

In this study, we provide a detailed analysis of S_{Hmax} orientations from stress related drilling-induced borehole failures, and assess their variability within the upper plate of the HSM. We analyze six borehole image and oriented four-arm caliper logs (not previously used for stress orientation studies), and provide a re-analysis of the seven borehole image logs investigated in Heidbach et al. (2018), Lawrence (2018), Griffin (2019), and Griffin et al. (2021) with a focus on ac-

quiring higher resolution measurements (length, width, orientation) of induced borehole features. We then discuss spatial variations in contemporary S_{Hmax} orientations and their relationship to far-field stresses and long-term patterns of tectonic deformation, and their potential links to along-strike variations in subduction megathrust slip behavior.

2 Geological Setting

The Hikurangi Subduction Margin (HSM) lies along the Pacific-Australian plate boundary at the southern end of the Tonga-Kermadec Trench, off the east coast of the North Island, New Zealand (Figure 1a). The Hikurangi Subduction Margin accommodates westward subduction of the Hikurangi Plateau (a Cretaceous large igneous province) beneath the continental crust of North Island at the Hikurangi Trough (Davy, 1992). The Hikurangi Plateau is ~10-15 km thick and transitions to a more typical 5-7 km thick oceanic plate further north at the Kermadec Trench (Davy et al., 2008; Davy, 1992; Ghisetti et al., 2016; Mochizuki et al., 2019). The southern termination of the HSM is located somewhere beneath New Zealand's northeastern South Island, where oblique convergence is transferred to the Marlborough Fault System and Alpine Fault in the South Island (Barnes et al., 1998; Little & Roberts, 1997).

Three major tectonic phases during the Neogene to present-day have been identified: 1) an early to middle Miocene compressional stage that resulted in extensive reverse faulting, folding, and tectonic uplift along the margin (Chanier et al., 1999; Barnes et al., 2002; Bailleul et al., 2013); 2) a mixed compressional and extensional stage from the mid-Miocene to early Pliocene resulting in widespread compressional tectonics and localized subsidence and normal faulting in the inner portion of the subduction wedge (Hawke's Bay region) (Barnes et al., 2002); 3) a compressional stage associated with and structural inversion of listric thrust faults and folds during the Quaternary and rapid, late Quaternary uplift of the Coastal Ranges, Axial Ranges, and Raukumara Peninsula (Beanland & Haines, 1998; Nicol et al., 2002, 2007; Nicol & Beavan, 2003; Bailleul et al. 2013). Late Quaternary extensional faulting in the Raukumara Peninsula is likely the result of gravitational collapse due to rapid uplift (Berryman et al., 2009; Pettinga, 2004; Walcott, 1987).

Neogene to present tectonic deformation across the HSM is complex and includes contributions from shortening associated with subduction at the Hikurangi Trough, clockwise rotation of the East Coast forearc, strike-slip faulting along the North Island Dextral Fault Belt (NIDFB), and back-arc extension in the Taupo Volcanic Zone (TVZ) (Beanland & Haines, 1998; Wallace et al., 2004; Figure 1a). The East Coast forearc has rotated for at least the last few Myr at rate of 3°–4°/Myr relative to the Australian plate (Nicol et al. 2007). This rotation results in back-arc rifting in the central North Island's Taupo Volcanic Zone (TVZ), transpression in the southern North Island, and creates a large along-strike change in convergence rate at the Hikurangi Trough, from 20 mm/year in the south to 60 mm/year at the northern Hikurangi Trough (Wallace et al. 2004; Figure 1a). Wallace et al. (2004) suggest that an along-strike change from

subduction of the large igneous province (Hikurangi Plateau) at the Hikurangi Trough, to normal oceanic crust along the Kermadec Trench exerts a torque on the forearc, producing clockwise rotation of the eastern North Island. Overall, relative motion between the Pacific and Australian plates occurs through this region at ~40 mm/yr, and is oblique to the orientation of the plate boundary. The oblique relative motion is partitioned into a margin-perpendicular component and a margin-parallel component. The margin-perpendicular component occurs along the Hikurangi subduction interface and provides a NW-SE shortening which is accommodated via the subduction interface and active thrust faults within the accretionary wedge and overriding plate (Barnes et al., 1998; Nicol and Beavan, 2003). The margin-parallel component is largely accommodated by a combination of right-lateral strike-slip on the North Island Dextral Fault Belt (NIDFB) and vertical-axis clockwise rotation of the North Island forearc (Beanland & Haines, 1998; Nicol et al., 2007; Wallace et al., 2004).

3 Data and Methodology

We analyze borehole image logs acquired from eleven boreholes using a range of tools including; the Schlumberger Fullbore Formation Microimager (FMI™; Figure 2a) and Oil Based Mud Imaging tool (OBMI™), Baker Atlas Simultaneous Acoustic and Resistivity Imager (STAR™), Tiger Energy Services Acoustic Formation Imaging Technology (AFIT; Figure 2b), and two orientated four-arm caliper logs (Figure 2c). The tool types and their borehole wall coverage for each borehole are summarized in Table 1.

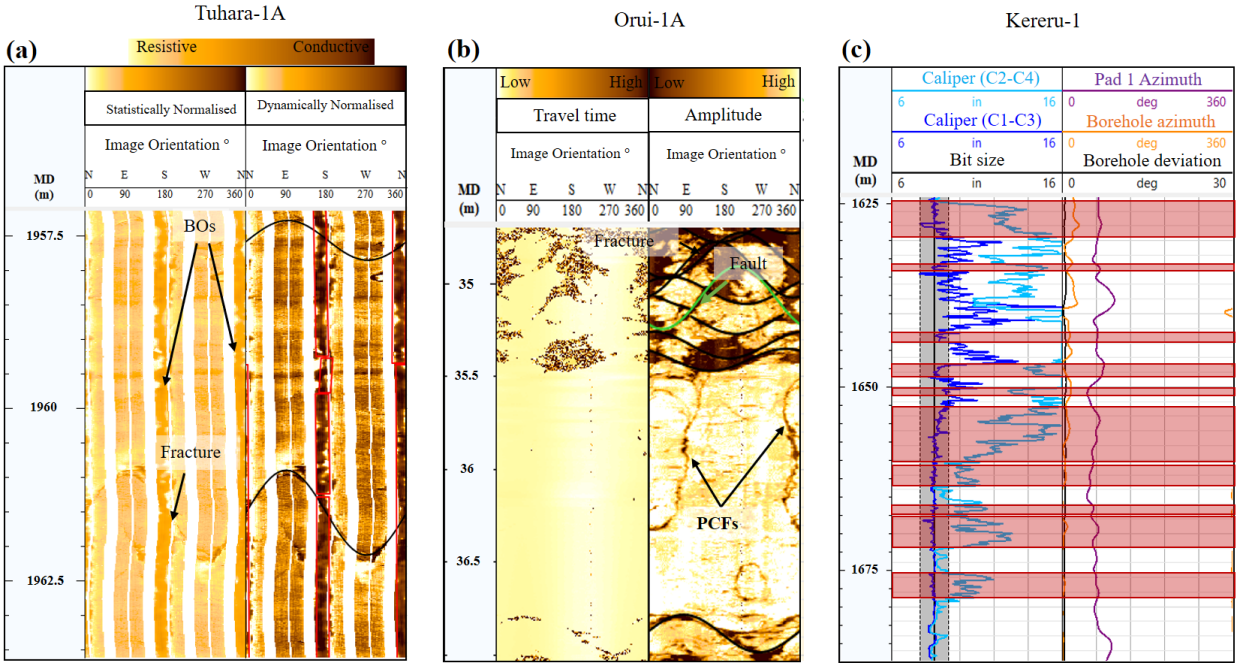

Figure 2. (a) Statically and dynamically normalized resistivity image log (FMI) showing borehole breakouts and natural fractures in borehole Tuhara-1A, (b) Dynamically normalized travel time and amplitude images from an acoustic image log (AFIT) acquired in Orui-1A borehole showing petal centerline fractures (PCFs), natural fractures, and a fault (observable offset of other geological features across a natural fracture). (c) Plot of an oriented four-arm caliper log (C1-C3 and C2-C4) from borehole Kereru-1. The 10% tolerance of bit size (black line) is shown as a grey shaded zone, plotted next to pad 1 azimuth and borehole orientation information showing caliper enlargement indicative of the presence of a borehole breakout.

Image log acquisition, data processing, and quality assessment is performed on all image logs, the details of which are documented in the supplemental information (Text S1 & S2).

From the borehole image logs, we identify stress-induced borehole failures, including borehole breakouts (BOs; Figure 2a & 2c), drilling-induced tensile fractures (DITFs), and petal-centerline fractures (PCFs; Figure 2b). BOs and DITFs are well-known indicators of horizontal in-situ stress orientations in vertical to semi-vertical boreholes, in which it is assumed one of the principal stresses is the vertical stress (S_v). BOs and DITFs develop parallel to the contemporary minimum (S_{hmin}) and maximum (S_{Hmax}) horizontal stresses respectively (Bell, 2003; Bell & Gough, 1979; Aadnoy & Bell, 1998). In such cases, BOs and DITFs can also be used to determine S_{Hmax} orientations in boreholes deviated $\geq 20^{\circ}$ as long as corrections are applied to address the impact of vertical stress (S_v) on their development (Peška & Zoback, 1995). BOs form as enlargements of the borehole diameter on opposite sides of the borehole wall where the circumferential hoop stress, induced by non-uniform horizontal principal stress magnitudes, is large enough to exceed the rock strength (Bell & Gough, 1979; Zoback, 2007). Borehole breakouts typically appear on resistivity image logs as a pair of wide, conductive (in water-based mud) or resistive (in oil-based mud, such as OBMI tool; King et al., 2010) zones. In acoustic televiewer logs, they appear as low amplitude, out-of-focus zones (Figure 2a). In both types of logs, BOs are located ~180° from each other around the circumference of the borehole wall. BOs often correlate with borehole enlargement and associated large caliper values as the result of the borehole failure (Figure 2c; Tingay et al., 2008). Oriented four-arm caliper data is also used to infer the presence of BOs along boreholes. To reliably distinguish BOs from other non-stress related features that affect borehole shape, such as keyseats and washouts, we apply the criteria presented by Reinecker et al., (2003).

DITFs develop on the borehole wall where there is a significant difference between the two horizontal principal stress magnitudes and the local stress concentrations around the borehole wall lead to hoop stresses that overcome the tensile strength of the rock (Brudy & Zoback, 1999; Zoback, 2007; Barton & Moos, 2010). DITFs typically appear as narrow, conductive (on resistivity image logs) or low amplitude and longer travel time (on acoustic image logs) pairs,

~180° from each other around the circumference of the borehole wall. DITFs are generally parallel or slightly inclined to the borehole axis in vertical to semi-vertical boreholes (Barton et al., 1998; Bell, 2003; Tingay et al., 2008; Rajabi et al., 2016a, 2016b). In this study, all BOs and DITFs are reported as individual feature length and width, such that a single BO or DITF measurement does not span a number of separate individual BOs or DITFs, similar to what has been done in previously analyzed HSM image logs (Lawrence, 2018; Griffin, 2019). This is an important aspect of quantifying induced features from borehole image logs because geological properties, such as varying strength associated with variably bedded lithologies, impact the development and growth (both width and length) of borehole breakouts (Kingdon et al., 2016; Fellgett et al., 2019). It is also important to capture each induced feature individually for accurate statistical considerations of borehole stress orientations.

PCFs are induced fractures that form within the bedrock ahead of the drill bit in response to stress concentrations at the bottom of the borehole during drilling, and propagate inward towards the borehole (Li & Schmitt, 1998; Davatzes & Hickman, 2010; Wenning et al., 2017). PCFs appear as conductive (resistivity image logs) or low amplitude (acoustic image logs) partial sinusoids that merge into discontinuous borehole axial centerline fractures (Figure 2b; Kulander et al., 1990). The average of the centerline fracture orientations or dip orientation of the partial sinusoids of a PCF is parallel to the orientation of S_{hmin} (Davatzes & Hickman, 2010). In contrast to the DITFs, the centerline portions of PCFs are often less than 180° apart from each other around the circumference of the borehole wall.

Finally, we use the A–E World Stress Map (WSM) quality ranking system and circular statistical analysis for stress orientation indicators (Heidbach et al., 2016). The borehole locations, image log intervals, S_{Hmax} orientation mean, standard deviation, and the quality classification are based on the length-weighted method (Heidbach et al., 2016) for individual boreholes are summarized in Table 1 and Table 2.

4 Results

4.1 Central HSM (Hawke's Bay region)

A total of 810 BOs with a combined length of 454 m are identified from borehole image logs and oriented four-arm caliper logs acquired in Kauhauroa-2, Kauhauroa-5, Makareao-1, Tuhara-1A, Kereru-1, and Whakatu-1 boreholes in the Central HSM region (Figure 3; data set 1; see Fig. 5 for the borehole locations and names). Using only BOs from boreholes with B-C quality rankings (following the WSM criteria), and so more likely to display far-field stress orientation measurements, a dominant 157°/337° ± 18° orientation is observed, indicating a NW-SE S_{hmin} orientation, from which we infer an S_{Hmax} orientation of 067°/247° (ENE-WSW) (Figure 3). The only exception is borehole Whakatu-1 (WSM D quality ranking), in the southeast area of the central HSM, which shows a dominant BO orientation of 054°/234° ±13° (NE-SW), from which we

infer a NW-SE S_{Hmax} orientation (144°/324°) (Table 1; Figure 3). 2 DITF pairs are observed in boreholes Kauhauroa-5 and Tuhara-1A with mean S_{Hmax} orientation of 020°/195° (NNE-SSW) and 079°/263° (ENE-WSW), respectively (Figure 3). No BOs, DITFs, or PCFs are observed in Waitahora-1 borehole from OBMI image logs (this image log only provided ~37% coverage of borehole wall) or from oriented four-arm caliper data.

Table 1. *Stress Indicators From Analysis of Borehole Image Logs and Oriented Four-Arm Caliper Data in the Central HSM, New Zealand.*

	Borehole ID	Max borehole Deviation (°)	Tool name	Borehole coverage (%)	Image interval (m MD)	Feature type	Number	Mean S_{Hmax}(°)	S.D	Total length (m)	Quality
Northern central HSM	**Kauhauroa-2**		FMI^{TM}		2138.5	BO		°/249°			C
	Kauhauroa-5		FMI^{TM}		1750.2	BO DITF	1	°/232°- 020°/195°		3.1	B D
	Makareo-1		FMI^{TM}		939.7	BO		°/238°			B
	Tuhara-1A		FMI^{TM}		2148	BO DITF	1	°/251°- 079°/263°		0.16	B D
Southern central HSM	**Kereru-1**		- arm caliper		1920	BO		°/259°			C
	Whakatu-1		- arm caliper		1400	BO		°/324°			D

Note. S_{Hmax} azimuth means, standard deviations (S.D.), and data quality ranking are calculated according to World Stress Map conventions (Heidbach et al., 2016).

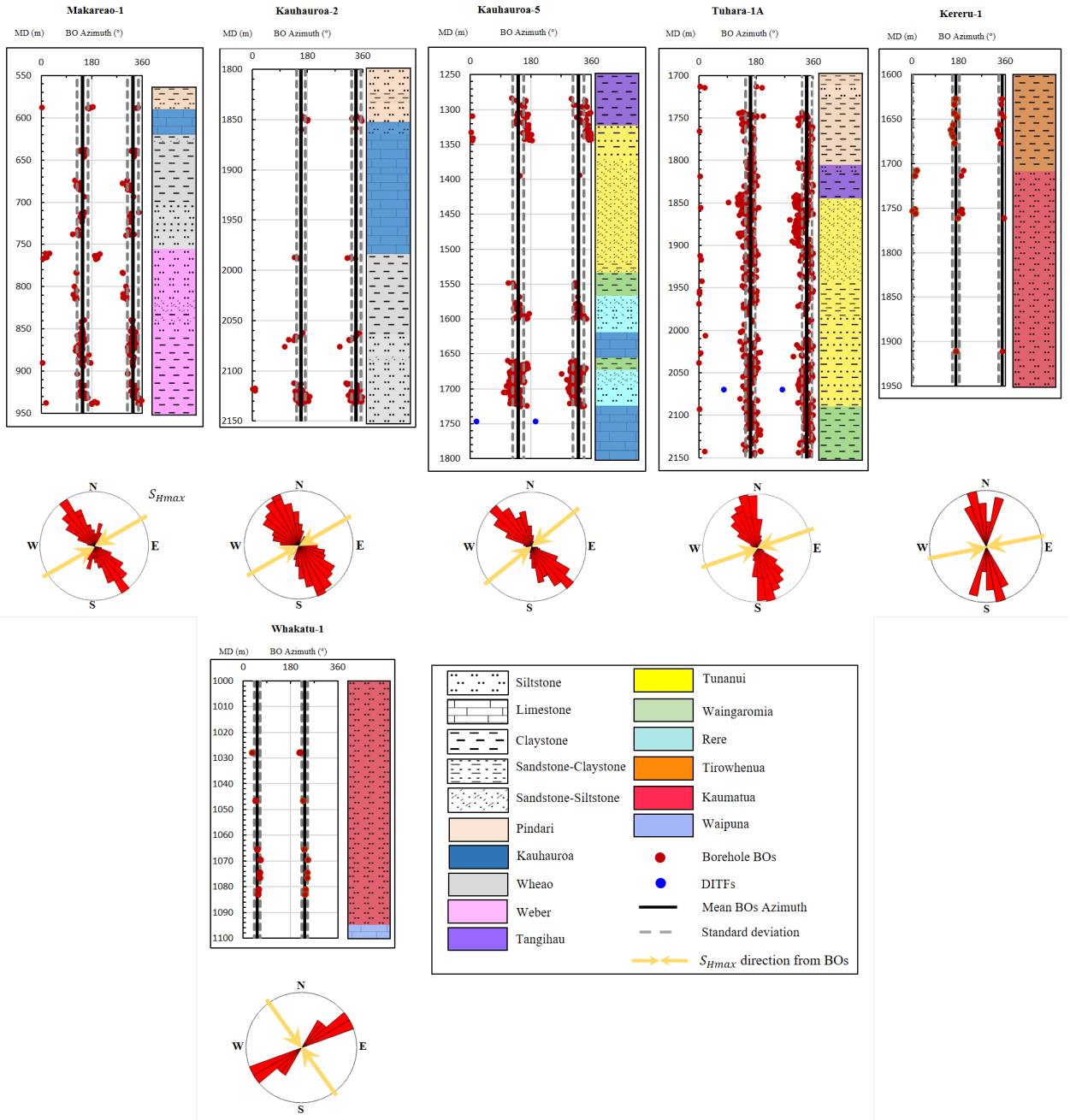

Figure 3. Graph of BO azimuths (red dots), DITF azimuths (blue dots), and stratigraphy column against measured depth (m MD) for boreholes at the central HSM. Mean BO azimuths and the standard deviation for individual borehole are plotted in black and dashed grey lines respectively. Bi-directional rose

diagram of breakout orientations for each borehole is shown below BO panels.

4.2 Southern HSM

A total of 1517 BOs with a combined length of 520 m are identified from borehole image logs in boreholes Ngapaeruru-1, Rauni-2, Titihaoa-1, Tawatawa-1, Te Mai-2, and Orui-1A boreholes (Figure 4; data set 1). For borehole stress data with a WSM quality ranking of B-C (Ngapaeruru-1, Tawatawa-1, and Ranui-2) we observe an S_{hmin} orientation of 016°/196° ± 21° (NNE-SSW) from which we infer an S_{Hmax} orientation of 106°/286° (WNW- ESE) (Figure 4). BOs in boreholes Ngapaeruru-1, Tawatawa-1, Te Mai-2, and the shallow (<1130 m MD) interval of Ranui-2 show a consistent WNW-ESE S_{Hmax} orientation (Figure 4), whereas BOs measured in boreholes Titihaoa-1, the deeper (>1130 m MD) imaged interval of Ranui-2, and Orui-1A provide dominantly NW-SE S_{Hmax} orientations (Figure 4). Our reanalysis of BOs from borehole Ranui-2 suggest a 51° clockwise S_{Hmax} orientation rotation from E-W (094°/274° ± 17°) in the shallower imaged depth interval (842-1130 m MD) to NW-SE (145°/325° ± 16°) in the deeper imaged interval (1130-1422 m MD) (Table 2) that was first reported by Griffin (2019).

Table 2. *Stress Indicators From Analysis of Borehole Image Logs in the Southern HSM, New Zealand.*

	Borehole ID	Max borehole deviation (°)	Tool name	% Borehole surface coverage	Image interval (m MD)	Feature type	Number	Mean S_{Hmax} (°)	S.D (°)	Total length (m)	Quality
Southern HSM	**Ngapaeruru-1**	17.78	FMI^{TM}		- 1417	BO		°/292°			B
	Rauni-2*	- 25.4	FMI^{TM}		- 1130	BO		°/274°16		49	B
					1130-1422	BO		145°/325°			B
	Te Mai-2		AFIT^{150}		- 147.5	BO		°/289°			D
	Orui-1A		AFIT^{150}		- 114.5	BO	1	°/335°-		0.8	D
						PCF	1	125° -		0.2	C
						DITF		133/295°			D
	Titihaoa-1		FMI^{TM}		- 2741	BO		°/332°			D
	Tawatawa-1		STAR		- 1540	BO		°/283°			B

Note. S_{Hmax} azimuth means, standard deviations (S.D.), and data quality ranking are calculated according to World Stress Map conventions (Heidbach et al., 2016). *Measured stress feature orientatioind are not corrected for borehole deviations$\geq 20^{\circ}$.

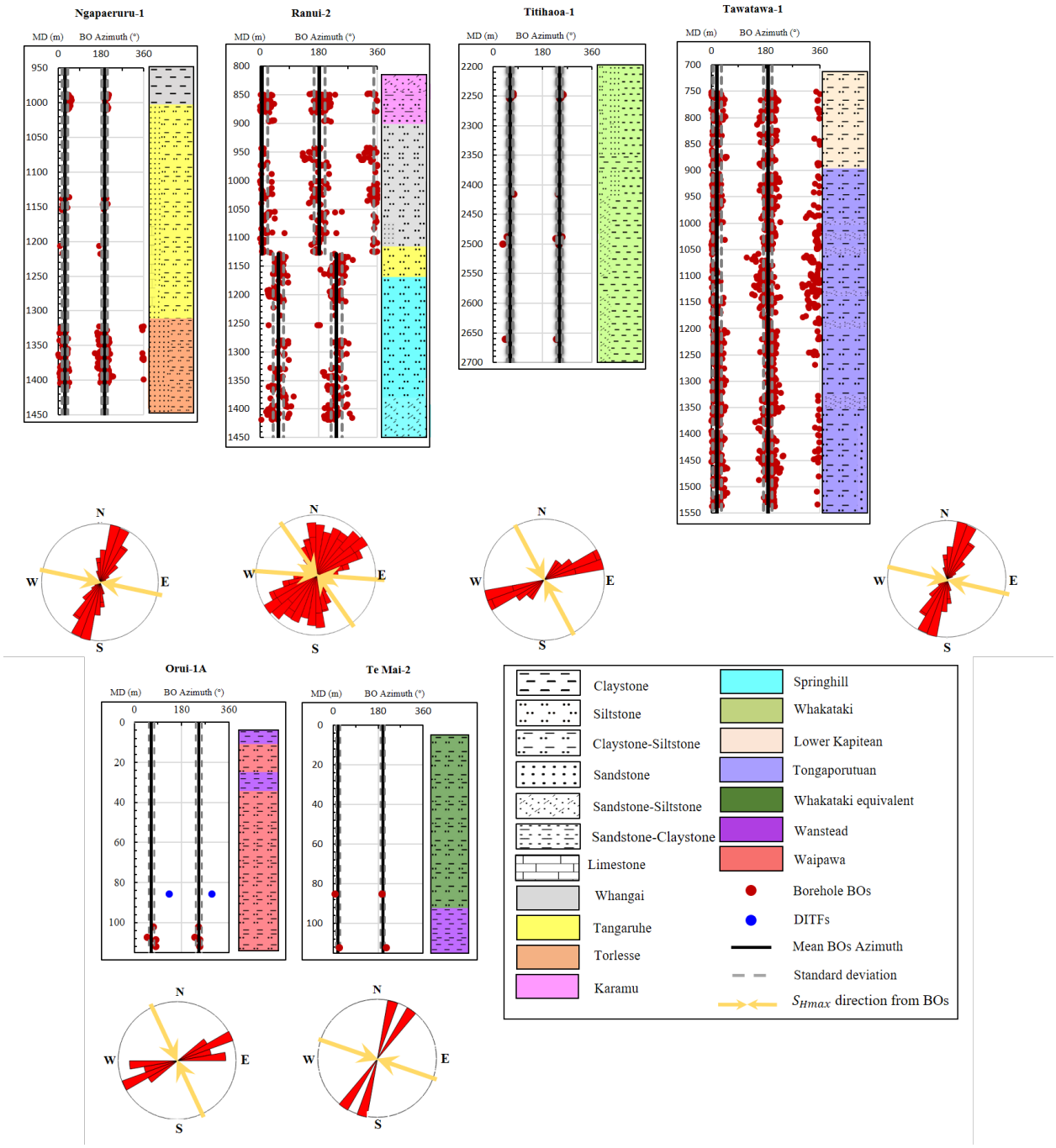

Figure 4. Graph of BO azimuths (red dots), DITF azimuths (blue dots), and stratigraphy column against measured depth (m MD) for boreholes at the south-

ern HSM. Mean BO azimuths and the standard deviation for individual borehole are plotted in black and dashed grey lines respectively. Bi-directional rose diagram of breakout orientations for each borehole is shown below BO panels.

5 Discussion

Our results show that the contemporary S_{Hmax} orientations in the upper plate of the HSM change from dominantly NE-SW, parallel to the subduction margin, within the central HSM to WNW-ESE/NW-SE within the southern HSM (Wairarapa region), roughly perpendicular to the subduction margin (Figure 5). This along-strike rotation in HSM S_{Hmax} orientations may be explained in a few ways; 1) HSM kinematics, 2) long-term tectonic deformations, and 3) lateral variations in basement topography.

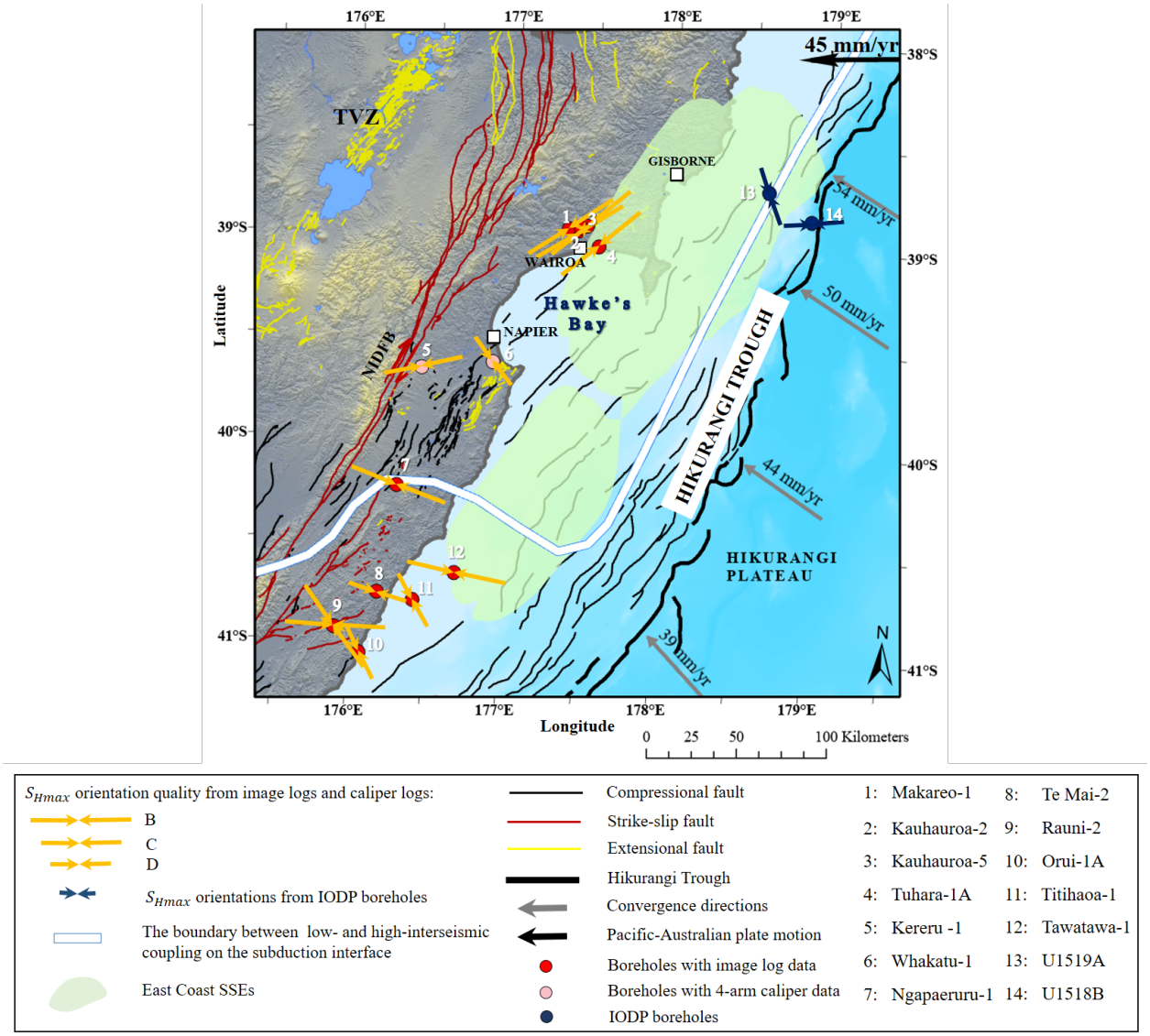

Figure 5. Map of S_{Hmax} at the East Coast of North Island determined from borehole Breakouts in (orange arrows) and IODP borehole image analysis from McNamara et al., 2021 (blue arrows). Green shaded region represents the East Coast cumulative slow slip (Wallace et al., 2012a). Active faults (normal faults: yellow; strike slip: red; reverse fault: black) traces from Litchfield et al. (2014) and Langridge et al, (2016). The bold black line shows the Hikurangi Through. Black arrow indicate the relative convergence vector between the Pacific and Australian Plates from DeMets et al., (1994) and grey arrows show shortening rates at the Hikurangi Trough from Wallace et al. (2012). Abbreviations:

NIDFB, North Island Dextral Fault Belt; TVZ, Taupo Volcanic Zone.

Geodetic measurements over the last 25 years have been used to determine New Zealand's contemporary surface strain field (Dimitrova et al., 2016; Haines &Wallace, 2020). The rotation of borehole-derived S_{Hmax} orientations along the HSM in the upper plate is remarkably consistent with the variation in coupling behavior on the HSM subduction interface (Figure 1b) and the along-strike rotation observed in the maximum contraction directions determined from geodetic measurements along the HSM forearc (Dimitrova et al., 2016; Haines & Wallace, 2020; Figure 6a). Maximum contraction directions determined from campaign GPS data reveal that the central HSM has a dominant E-W maximum contraction direction, whereas the southern HSM shows a NW-SE contraction direction (Figure 6a; Haines & Wallace, 2020), broadly compatible with the borehole-derived S_{Hmax} orientations reported here. The along-strike variations in maximum contraction directions from GPS are suggested to be related to along-strike changes in interseismic coupling on the HSM plate interface (Wallace et al., 2004; Dimitrova et al., 2016). In the northern and central HSM, the subduction interface is largely creeping and experiences shallow (<15 km), episodic slow slip events on the offshore. At the southern HSM the plate interface is strongly interseismically coupled to ~30 km depth, and is currently accumulating elastic strain in the surrounding crust that will eventually be relieved in future large earthquakes (Wallace, 2020; Figure 1b). The strong agreement between the geodetic maximum contraction directions and the observed stress field from the borehole observations indicate that S_{Hmax} orientations and their variability at HSM are strongly influenced by along-strike variations in elastic strain accumulation in the overriding plate due to changes in interseismic coupling on the subduction interface.

In the central HSM (where the plate boundary is largely creeping) borehole-derived S_{Hmax} orientations and maximum contraction directions are reasonably consistent and sub-parallel to far-field relative Pacific-Australian plate motion. In contrast, at the southern HSM borehole-derived S_{Hmax} orientations and maximum contraction directions are roughly perpendicular to far-field relative Pacific-Australian plate motion, but are parallel to the convergence direction. This observation may be due to the fact that the subducting plate drags the forearc wedge in the direction of subduction and increases elastic compression strain and stress on the plate interface and within the forearc itself aligning elastic strain accumulation and S_{Hmax} stress orientations into that orientation. These S_{Hmax} orientation observations are at odds with those of Townend and Zoback (2006) showing that stress orientations in central Japan (from earthquake focal mechanisms) do not agree with maximum contraction directions associated with cyclical subduction zone locking. This difference in the conclusions between our study and Townend and Zoback (2006) may be related to the fact that we utilize shallow (<3 km) stress orientations, which may be more susceptible to temporal changes in elastic strain resulting from interseismic coupling rather than stress orientations from earthquake focal mechanisms sampling greater depths. This observation at the HSM may be reflecting longer-term ac-

cumulation of stress (related to long-term tectonic processes) independent of stage within the earthquake cycle.

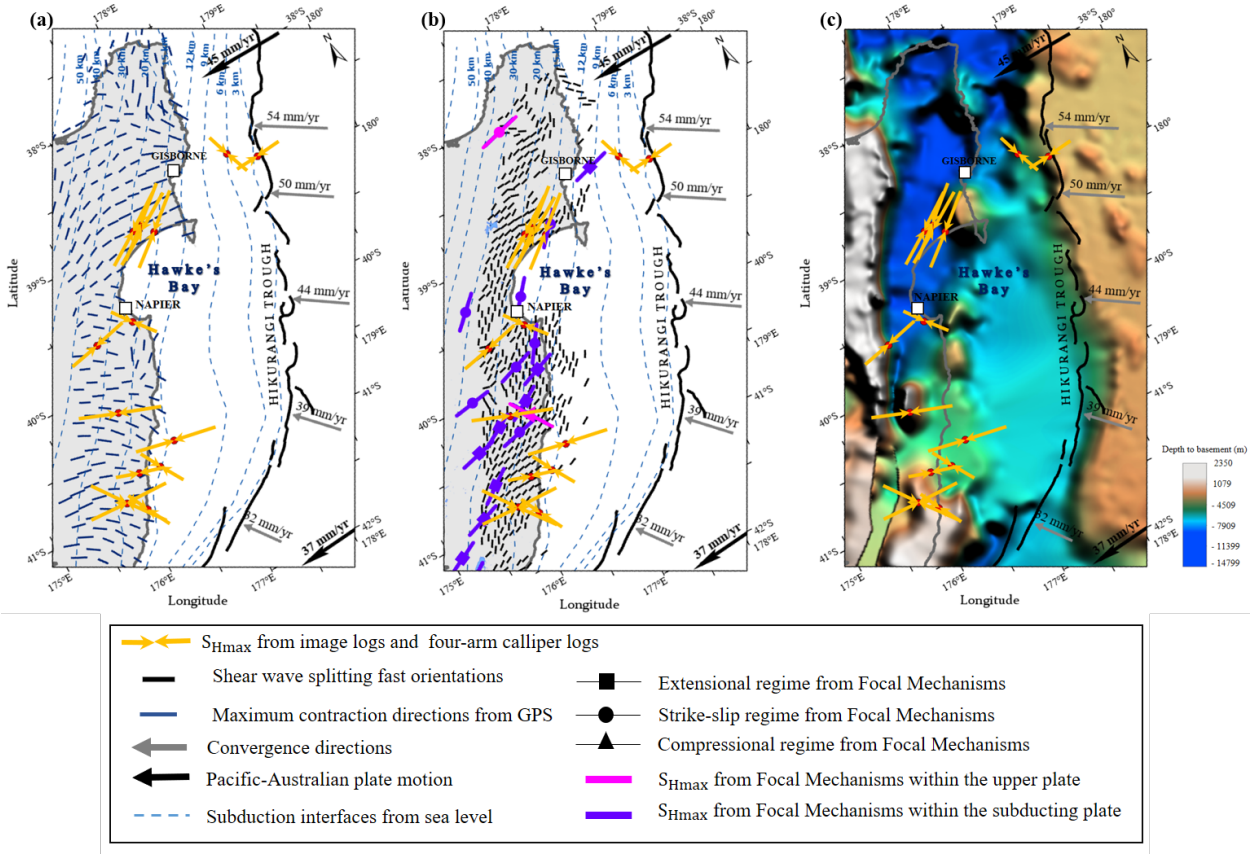

Figure 6. (a) Map of maximum contraction directions from GPS data (Haines & Wallace, 2020) and borehole-derived S_{Hmax} orientations (orange arrows) and IODP borehole image analysis from McNamara et al. (2021) (blue arrows). (b) Map of S_{Hmax} orientations and inferred faulting regime from focal plane mechanisms (0-60 km; square: extensional, circle: strike-slip, and triangle: compressional regime; Townend et al., 2012), seismic anisotropy measurements (0-40 km; black lines). Dashed blue lines show depth of subduction interface from sea level (Williams et al., 2013). (c) The map showing depth to basement map of North Island adapted from FROGTECH (2014). The clockwise rotation of S_{Hmax} orientation along the HSM strike follows the basement topography. Black arrows indicate the long-term motion of the Pacific relative to Australian Plate from DeMets et al., (1994) and grey arrows show shortening rates at the Hikurangi Trough from Wallace et al. (2012). Red dots show the borehole locations.

Although borehole-derived S_{Hmax} orientations at the HSM are broadly consistent with maximum contraction directions, S_{Hmax} orientations are not uniform

within the forearc and in places deviate from the observed maximum contraction directions (Figure 6a). Some of these variabilities may be due to longer-term partitioning of oblique relative motion and strain into margin-parallel, margin-perpendicular, and strike-slip components. Similar deviations from maximum contraction directions are observed within the Nankai subduction zone (Chang et al., 2010) and Costa Rica margin (Malinverno et. al, 2016). For example, borehole-derived S_{Hmax} orientations in the accretionary prism across the Nankai subduction zone are subparallel to the plate convergence vector between the Philippine Sea plate and Japan, perpendicular to the plate boundary, and for one borehole in the shelf edge is parallel to the plate boundary (Lin et al., 2010; Chang et al. 2010; Wu et al. 2012). The variations of stress among these sites and the deviation of borehole-derived S_{Hmax} orientations from the plate motion vectors derived from GPS data are suggested to be attributed to the strain partitioning into trench-parallel, right-lateral slip and thrust tectonics due to oblique plate convergence (Tobin et al. 2009; Lin et al. 2010). Alternatively, such stress variations have also been attributed to other factors such as thrusting and bending within individual geologic domains and local extension deformations derived by gravitation collapse of the prism in the forearc (Chang et al., 2010; Lin et al., 2016).

Townend et al. (2012) derived S_{Hmax} orientations from earthquake focal mechanisms using a Bayesian approach for earthquake data between 2004-2011 with $M_L > 3$. Their observations reveal that S_{Hmax} orientation changes from NE-SW in the central HSM to a more oblique S_{Hmax} orientation, sub-parallel to Pacific-Australia relative plate motion, in the southern HSM (Figure 6b). Only two focal mechanism solutions are located within the upper plate of the HSM or near the subduction interface; one strike-slip event with a NE-SW S_{Hmax} orientation (latitude 38°S; North of central HSM) at 7 km depth, and one compressional event with a WNW-ESE S_{Hmax} orientation (latitude 40.5°S; southern HSM) at 25 km depth (at the top of subducting plate near the subduction interface; Figure 6b). In the central HSM (where the plate boundary is largely creeping) borehole-derived NE-SW S_{Hmax} orientations and maximum contraction directions agree with the NE-SW S_{Hmax} orientations derived from focal mechanism inversions within the upper plate and subducting plate, implying that far-field plate boundary forces exerted at the HSM primarily control the present-day crustal stresses in the upper plate in this area. In contrast, the southern HSM shows stress field rotation with depth from borehole-derived WNW-ESE/NW-SE S_{Hmax} orientations (roughly margin-perpendicular) in the shallow crust of upper plate to NE-SW/ ENE-WSW focal mechanism-derived S_{Hmax} orientations within the subducting plate (Figure 6b). The NE-SW/ ENE-WSW S_{Hmax} orientations derived from focal mechanism inversions indicate a normal or strike-slip tectonic regime within the subducting plate of the southern HSM. There is one compressional event at ~25 km depth (near the subduction interface) where the borehole-derived S_{Hmax} orientation agrees with a focal mechanism-derived WNW-ESE S_{Hmax} orientation (latitude 40.5°S; Figure 6b). This implies that the overriding plate broadly is in a condition of horizontal compression parallel

to convergence direction, potentially as deep as the plate interface (±10 km) (barring localized variations) and the tectonic regime becomes more strike-slip and normal within the subducting plate. The change in stress orientation with depth in the southern HSM is more compatible with a theoretically mechanically weak plate interface with low resolved shear stress and normal effective stress on the plate interface. The fact that the upper plate is in the state of horizontal compression parallel to plate convergence, on the other hand, implies that contemporary S_{Hmax} orientation is being driven by subduction of Hikurangi Plateau beneath North Island. Taking these observations into consideration, we propose that plate interface remains mechanically weak along the whole HSM and that a small increase of elastic compression strain and stress caused by the interseismically coupled southern HSM interface is sufficient to rotate S_{Hmax} orientation in the upper plate toward the subduction direction.

More recently, Illsley-Kemp et al. (2019) measured seismic anisotropy using shear wave splitting fast orientations from earthquake data in 2005–July 2018 with $M_L>0$. Some studies consider fast orientations as a proxy for S_{Hmax} orientation if other significant crustal anisotropies are not present (e.g. fracturing, faulting, grain and crustal preferred orientations). The seismic anisotropy was derived from events 40 km deep and fast orientations were dominantly NE-SW (margin-parallel) for most of the HSM forearc, and more ENE-WSW in the northern and central HSM (Figure 6b). With the exception of some portions of the central HSM, the fast directions from shear-wave splitting studies do not agree well with the S_{Hmax} orientations we measure in the shallow boreholes. This could mean either (a) that the shear wave splitting fast directions are not controlled by contemporary S_{Hmax} orientation, or (b) that the fast directions are mainly controlled by structural features such as faults and the stress state at greater depths, which may be different than the near-surface which our study samples. In fact, propagating waves sample the volume of crust above the hypocenter without taking the variation of anisotropic with depth into account.

Long-term tectonic deformation resulting from rapid clockwise rotation of the Hikurangi forearc (Wallace et al. 2004) may also possibly explain the along-strike variation in S_{Hmax} orientation. The clockwise rotation of forearc, which accommodates the margin-parallel component of oblique Pacific-Australian plate motion, results in significant tectonic transitions along the strike (Nicol et al., 2007; Wallace et al., 2004). Tectonic regime varies from back-arc rifting within the TVZ in the central part of North Island, strike-slip and normal faulting onshore of the northern and central HSM to transpression and reverse faulting at the southern HSM (Figure 5). The rotation of S_{Hmax} orientations from margin-parallel in the onshore central HSM to margin-perpendicular in the southern HSM likely reflects this transition in the tectonic regime, Such that the NE-SW S_{Hmax} orientation in the central HSM reflects margin-normal extension due to the transmission of slab rollback forces across the forearc and into the adjacent extensional back-arc rift (Wallace et al., 2012b). The clockwise rotation of the Hikurangi forearc may also explain why our observed contemporary S_{Hmax} orientation of NE-SW is not consistent with active large-scale NE-SW striking

compressional faults in the central HSM. The imaged intervals of the central HSM boreholes are located within the hanging walls of active NE-SW striking compressional faults and within NE-SW oriented fault-bend fold axes identified from seismic reflection profiles (Western Energy New Zealand, 2001; Barnes et al., 2002). It is possible that the deformation and growing rate of these reverse faults within the central HSM have changed through time, allowing forces exerted by forearc rotation surpass the NW-SE compression stress on these active faults. In this case, the rotation of the forearc, which accommodates the margin-parallel component, induces a NE slip motion on these pre-existing faults. This also suggests that these reverse faults in the context of current stress field could be currently active as strike-/oblique-slip faults. Another possibility is that due to frequent earthquakes in this region, the S_{Hmax} orientation within the central HSM has changed from a potential NW-SE orientation perpendicular to the margin, compatible with the orientation of observed reverse faults and fold axes, to the contemporary NE-SW orientation subparallel to the margin. During the interseimic period, strain and stress accumulation along the reverse faults and subduction interface drives compression in the upper plate parallel to convergence direction. Following great earthquakes or frequent earthquakes, the margin-perpendicular component is reduced due to post-seismic stress release, allowing a strike-slip motion in direction of long-term oblique relative plate motion on these faults. This implies that the stress state associated with seismicity perturbations is quite long lasting (these boreholes are drilled over the course of 4 years) such that stress state require a long time to recover or the perturbations were significant enough to permanently reorient the stress. In this scenario, the intermediate principal stress (S_{hmin}) and minimum principal stress (S_v) would switch and principal stresses re-orient in response to forces exerted by long-term relative plate motion and fluctuations in the magnitude of stress parallel to plate convergence, modulated by the seismic cycles. Sacks et al. (2013) and Moore et al. (2013) used a similar concept to explain the contrast between S_{Hmax} orientations and normal fault strikes within Kumano Basin of the Nankai subduction zone.

Lateral variations in surface and basement topography may also play a role in the observed along-strike variation in upper plate borehole-derived S_{Hmax} orientations (Figure 6c). Basement structures such as faults, folds, and seamounts that are not covered by thick sediments can cause significant stress rotation at both regional and large scales by introducing geomechanical inhomogeneities and lateral discontinuities (Gale et al., 1984; Enever et al. 1999; Rajabi et al., 2016a). In fact, the presence of seamounts on the incoming plate have been suggested as a possible localized effect on stress field orientations and shear-wave splitting fast directions in the offshore northern HSM (McNamara et al., 2021; Zal et al., 2020). The SEEBASE™ model of New Zealand, a depth to basement map based on the integrated interpretation of gravity, magnetic, borehole, and seismic data (Figure 6c) clearly shows a significant change in sediment thickness overlying the basement rocks, and basement topography along the HSM margin (FROGTECH , 2014). The onshore northern and central HSM basement is

located at depths ~9-15 km and covered by thick Neogene sediments, whereas at the onshore and offshore southern HSM the Mesozoic greywacke basement is uplifted and located at relatively shallow depths (<5 km), and in some locations above sea level. Thin sediment packages directly overlying mechanically strong basement rocks, may be more reflective of the tectonic stresses experienced by the basement. Hence, it is possible that the basement compressional structures striking NNE/NE-SSW/SW control the observed margin-perpendicular, NW-SE S_{Hmax} orientation within the shallow crust of the southern HSM.

In addition to large-scale stress variations, localized variations have been observed between and within individual boreholes which could be attributed to local active geological structures such as faults, surface topography, and variable mechanical properties. For instance a localized NW-SE S_{Hmax} orientation ($144° \pm 11°$) is noted from four-arm caliper data in borehole Whakatu-1 (south of Napier; Figure 5), perpendicular to the dominant NE-SW S_{Hmax} orientation of the central HSM. The NW-SE S_{Hmax} orientation in Whakatu-1 is margin-perpendicular implying a localized compressional tectonic regime at this locale, which agrees well with observed onshore and offshore active, NNE-SSW striking, compressional faults in this region (Figure 5; Litchfield et al. (2014); Langridge et al, (2016)), such as the reverse fault responsible for growth of the Cape Kidnapper's anticline (Hull, 1987). Furthermore, Dimitrova et al. (2016) reported a possible locked patch in southern central HSM between shallow SSEs on the East Coast and deep Kaimanawa SSEs west of the East Coast (Figure 1b). Downdip changes in interseismic coupling behavior of the subduction interface and the accumulated strain associated with the locked patch could also be influencing the compressional tectonic regime in this region and borehole Whakatu-1.

6 Conclusions

This paper presents the first comprehensive analysis of contemporary S_{Hmax} orientations along the HSM, and discusses stress field orientation variability within the context of variable tectonics and slip behavior of this subduction margin. S_{Hmax} orientations in the central HSM are predominately NE-SW (sub-parallel to plate boundary), which rotates to a dominantly WNW-ESE S_{Hmax} orientation in the southern HSM (approximately perpendicular to the plate boundary). Our borehole-derived S_{Hmax} orientations agree with the maximum contraction strain directions from GPS measurements along the HSM suggesting that the observed stress orientations along the HSM are influenced by elastic strain accumulation due to interseismic coupling on the Hikurangi subduction interface. The long-term tectonic deformation arising from rapid rotation of the Hikurangi forearc, causing reverse faulting and strike-slip in the southern part of the margin and a combination of extension and strike-slip in the northern and central margin and the basement topography may also be at play in influencing the along-strike variations in observed stress orientations. In the southern HSM, borehole-derived S_{Hmax} orientations are inconsistent with S_{Hmax} orientations derived from focal mechanism solutions in the subducting plate, implying that the southern HSM interface is mechanically weak. Further interpretation of

HSM stress state could be achieved by constraining stress magnitudes, which will be the focus of future studies.

Acknowledgments

This publication has emanated from research conducted with the financial support of Science Foundation Ireland (SFI) under Grant Number 17/RC-PhD/3481 and Geological survey of Ireland (GSI). The authors would like to thank the New Zealand Petroleum and Minerals group (NZPM) within the Ministry for Business, Innovation and Employment (MBIE) for providing access to borehole data and supporting materials for this study. We also thank Schlumberger for providing academic licenses for Techlog 2018.1 to University College Dublin and University of Liverpool. We thank to Esri for providing the academic license of ArcGIS Pro. For the purpose of Open Access, the author has applied a CC BY public copyright license to any Author Accepted Manuscript version arising from this submission.

Data Availability Statement

This research used data provided by the New Zealand Petroleum and Minerals group (NZPM) within the Ministry for Business, Innovation and Employment (MBIE). The borehole image logs and oriented four-arm caliper data used in this paper can accessed through MBIE 's database. All additional data used in this article was collected from published sources referenced in the text. In Supporting Information, data set 1 contains all borehole breakouts presented in this study.

References

Aadnoy, B. S., & Bell, J. S. (1998), Classification of drill-induce fractures and their relationship to in-situ stress directions. *The Log Analyst*, *39* (06), 27–42.

Bailleul, J., Chanier, F., Ferrière, J., Robin, C., Nicol, A., Mahieux, G., et al. (2013), Neogene evolution of lower trench-slope basins and wedge development in the central hikurangi subduction margin, new zealand. *Tectonophysics*, *591*, 152–174. https://doi.org/10.1016/j.tecto.2013.01.003

Barnes, P. M., Lamarche, G., Bialas, J., Henrys, S., Pecher, I., Netzeband, G. L., et al. (2010), Tectonic and geological framework for gas hydrates and cold seeps on the Hikurangi Subduction Margin, New Zealand. Marine Geology, 272(1–4), 26–48. https://doi.org/10.1016/j. margeo.2009.03.012

Barnes, P. M., Lpinay, M. De, Collot, J. Y., Delteil, J., & Audru, J.-C. (1998), Strain partitioning in the transition area between oblique subduction and continental collision, Hikurangi margin. *Tectonics*, *17*(4), 534–557.

Barnes, P. M., Nicol, A., & Harrison, T. (2002), Late Cenozoic evolution and earthquake potential of an active listric thrust complex above the Hikurangi subduction zone, New Zealand. *Bulletin of the Geological Society of America*, *114*(11), 1379–1405. https://doi.org/10.1130/0016-7606(2002)114<1379:LCEAEP>2.0.CO;2

Barton, C. A., Hickman, S., Morin, R., Zoback, M. D., & Benoit, D. (1998), Reservoir-scale fracture permeability in the Dixie Valley, Nevada, geothermal field. SPE/ISRM Rock Mechanics in Petroleum Engineering, Trondheim, Norway, July 1998, 47371, 315–322.

Barton, C., & Moos, D. (2010), Geomechanical wellbore imaging: Key to managing the asset life cycle, in M. Po¨ppelreiter, C. Garcı´a-Carballido, and M. Kraaijveld, eds., Dipmeter and borehole image log technology: *American Association of Petroleum Geologists Memoir*, *92*, 1–32. https://doi.org/10.1306/13181279M922689

Beanland, S., & Haines, J. (1998), The kinematics of active deformation in the North Island, New Zealand, determined from geological strain rates. *New Zealand Journal of Geology and Geophysics*, *41*(4), 311–323. https://doi.org/10.1080/00288306.1998.9514813

Bell, J. S. (2003), Practical methods for estimating in situ stresses for borehole stability applications in sedimentary basins. *Journal of Petroleum Science and Engineering*, *38*(3–4), 111–119. https://doi.org/10.1016/S0920-4105(03)00025-1

Bell, J. S., & Gough, D. I. (1979), Northeast-southwest compressive stress in Alberta evidence from oil wells. *Earth and Planetary Science Letters*, *45*(2), 475–482. https://doi.org/10.1016/0012-821X(79)90146-8

Berryman, K., Marden, M., Palmer, A., & Litchfield, N. (2009), Holocene rupture of the Repongaere fault, Gisborne : Implications for Raukumara Peninsula deformation and impact on the Waipaoa Sedimentary System Holocene rupture of the Repongaere Fault, Gisborne : and impact on the Waipaoa Sedimentary System. *New Zealand Journal of Geology and Geophysics*, *52*(4), 335–347. https://doi.org/10.1080/00288306.2009.9518462

Brodsky, E. E., Saffer, D., Fulton, P., Chester, F., Conin, M., Huffman, K., et al. (2017), The postearthquake stress state on the Tohoku megathrust as constrained by reanalysis of the JFAST breakout data. *Geophysical Research Letters*, *44*, 8294–8302. https://doi.org/10.1002/2017GL074027

Brudy, M., & Zoback, M. D. (1999), Drilling-induced tensile wall-fractures: Implications for determination of in-situ stress orientation and magnitude. *International Journal of Rock Mechanics and Mining Sciences*, *36*, 191–215. https://doi.org/10.1016/S0148-9062(98)00182-X

Byrne, T. B., Lin, W., Tsutsumi, A., Yamamoto, Y., Lewis, J. C., Kanagawa, K., et al. (2009), Anelastic strain recovery reveals extension across SW Japan subduction zone Anelastic strain recovery reveals extension across SW Japan subduction zone. *Geophysical Research Letters*, *36*(L23310). https://doi.org/10.1029/2009GL040749

Chang, C., McNeill, L. C., Moore, J. C., Lin, W., Conin, M., & Yamada, Y. (2010), In situ stress state in the Nankai accretionary wedge estimated from borehole wall failures. *Geochemistry, Geophysics, Geosystems*, *11*(12), 1–17. https://doi.org/10.1029/2010GC003261

Chanier, F., Ferriere, J., & Angelier, J. (1999), Extensional deformation across an active margin, relations with subsidence, uplift, and rotations: The Hikurangi subduction, New Zealand. *Tectonics*, *18*(5), 862–876.

Davatzes, N. C., & Hickman, S. H. (2010), Stress, fracture, and fluid-flow analysis using acoustic and electrical image logs in hot fractured granites of the Coso geothermal field, California, U.S.A. In M. Po¨ppelreiter, C. Garcı´a-Carballido, and M. Kraaijveld, eds., Dipmeter and borehole image log technology (259–293). https://doi.org/10.1306/13181288M923134

Davy, B. W. (1992), The influence of subducting plate buoyancy on subduction of the Hikurangi-Chatham Plateau beneath the North Island, New Zealand. *Geology and Geophysics of Continental Margins*.

Davy, B., Hoernle, K., & Werner, R. (2008), Hikurangi Plateau: crustal structure, rifted formation, and Gondwana subduction history. *Geochemistry, Geophysics, Geosystems*, *9*(7). https://doi.org/10.1029/2007GC001855

DeMets, C., Gordon, R. G., Argus, D. F. & Stein, S. (1994), Effect of recent revisions to the geomagnetic reversal time scale on estimates of current plate motions. *Geophysical Research Letters*, *21*, 2191–2194.

Dimitrova, L. L., Wallace, L. M., Haines, A. J., & Williams, C. A. (2016), High-resolution view of active tectonic deformation along the Hikurangi subduction margin and the Taupo Volcanic Zone, New Zealand. *New Zealand Journal of Geology and Geophysics*, *59*(1), 43–57. https://doi.org/10.1080/00288306.2015.1127823

Enever, J. R., Gale, W. & Fabjanczvk, M. (1999), A study of the variability of the horizontal stress field in a sedimentary basin. *9th International Society for Rock Mechanics Congress*, Paris, France, 1257-1260.

Fellgett, M. W., Kingdon, A., Waters, C. N., Field, L., Shreeve, J.,

Dobbs, M., & Ougier-simonin, A. (2019), Lithological constraints on borehole wall failure ; a study on the Pennine coal measures of the United Kingdom. *Frontiers in Earth Science*, *7*(163). https://doi.org/10.3389/feart.2019.00163

FROGTECH. (2014), New Zealand Basement Composition and Heat Flow GIS Project. Report prepared for the Government of New Zealand, Department of Petroleum and Minerals.

Gale, W. J., Enever, J. R., Blackwood, R. L. & McKay, J. (1984), An investigation of the effect of a fault /monocline structure on the in-situ stress field and mining conditions at Nattai Bulli Colliery NSW, Australia. CSIRO Australia, Division of Geomechanics. Geomechanics of Coal Mining Report No. 48.

Ghisetti, F. C., Barnes, P. M., Ellis, S., Plaza-Faverola, A. A., & Barker, D. H. N. (2016), The last 2 Myr of accretionary wedge construction in the central Hikurangi margin (North Island, New Zealand): Insights from structural modeling. *Geochemistry, Geophysics, Geosystems*, *17*(11), 4517–4533. https://doi.org/10.1002/2016GC006341

Griffin, A. G. (2019), Subsurface S_{HMAX} determined from a borehole image log, onshore southern East Coast Basin, New Zealand. *New Zealand Journal of Geology and Geophysics*, *62*(2), 273–290. https://doi.org/10.1080/00288306.2019.1570946

Griffin, A. G., Bland, K. J., Morgans, H. E. G., Strogen, D. P. (2021), A multifaceted study of the offshore Titihaoa-1 drillhole and a Neogene accretionary slope basin , Hikurangi subduction margin. *New Zealand Journal of Geology and Geophysics*. https://doi.org/10.1080/00288306.2021.1932527

Haines, A. J., & Wallace, L. M. (2020), New Zealand-wide geodetic strain rates using a physics-based approach. *Geophysical Research Letters*, *47*(1). https://doi.org/10.1029/2019GL084606

Hardebeck, J. L. (2004), Stress triggering and earthquake probability estimates. *Journal of Geophysical Research*, *109*(B04310). http://dx.doi.org/10.1029/2003JB002437

Hardebeck, J. L., & Okada, T. (2018), Temporal stress changes caused by earthquakes: a review. *Journal of Geophysical Research : Solid Earth*, *123*, 1350–1365. https://doi.org/10.1002/2017JB014617

Heidbach, O., Barth, A., Müller, B., Reinecker, J., Stephansson, O., Tingay, M., & Zang, A. (2016), WSM quality ranking scheme, database description and analysis guidelines for stress indicator. World Stress Map Technical Report 16-01. GFZ German Research Centre for Geosciences. http://doi.org/10.2312/wsm.2016.001

Heidbach, O., Rajabi, M., Cui, X., Fuchs, K., Müller, B., Reinecker, J., et al. (2018), The world stress map database release 2016: crustal stress pattern across scales. *Tectonophysics*, *744*, 484–98. https ://doi.org/10.1016/j.tecto .2018.07.007

Huffman, K. A., & Saffer, D. M. (2016), In situ stress magnitudes at the toe of the Nankai Trough accretionary prism, offshore Shikoku Island, Japan. *Journal of Geophysical Research : Solid Earth*, *121*, 1202–1217. https://doi.org/10.1002/2015JB012415

Hull, A. (1987), A late holocene marine terrace on the kidnappers coast, north island , new zealand : some implications for shore platform development processes and uplift mechanism. *Quaternary Research*, *28*(2), 183–195.

Illsley-Kemp, F., Savage, M. K., Wilson, C. J. N., & Bannister, S. (2019), Mapping stress and structure from subducting slab to magmatic rift: crustal seismic anisotropy of the North Island, New Zealand. *Geochemistry, Geophysics, Geosystems*, *20*. https://doi.org/10.1029/2019gc008529

Jaeger, J., Cook, N., & Zimmerman, R. (2007), Fundamentals of rock mechanics. *Wiley-Blackwell*. https://doi.org/10.1017/CBO9780511735349

King, R. C., Tingay, M. R. P., Hillis, R. R., Morley, C. K., & Clark, J. (2010), Present-day stress orientations and tectonic provinces of the NW Borneo collisional margin. *Journal of Geophysical Research: Solid Earth*, *115*(10). https://doi.org/10.1029/2009JB006997

Kingdon, A., Fellgett, M. W., & Williams, J. D. O. (2016), Use of borehole imaging to improve understanding of the in-situ stress orientation of Central and Northern England and its implications for unconventional hydrocarbon resources. *Marine and Petroleum Geology*, *73*, 1–20. https://doi.org/10.1016/j.marpetgeo.2016.02.012

Kulander, B. R., Dean, S. L., & Ward Jr., B. J. (1990), Fractured core analysis: Interpretation, logging, and use of natural and induced fractures in core. American Association of Petroleum Geologists, 8, Tulsa, Oklahoma.Laird, M. G., & Bradshaw, J. D. (2004), The breakup of a long-term relationship : the Cretaceous separation of New Zealand from Gondwana. *Gondwana Research*, *7*(I), 273–286.

Langridge, R. M., Ries, W. F., Litchfield, N. J., Villamor, P., Van Dissen, R. J., Barrell, D. J. A., et al. (2016), The New Zealand active faults database. *New Zealand Journal of Geology and Geophysics*, *59* (1), 86–96. https://doi.org/10.1080/00288306.2015.1112818

Lawrence, M. J. F. (2018), Structural and Sedimentological Interpretation of Well Data from the Wairoa Area, North

Island, New Zealand. GNS Science Report 2018/28, 1–76. https://doi.org/10.21420/G23W81

Li, Y., & Schmitt, D. R. (1998), Drilling-induced core fractures and in situ stress. Journal of Geophysical Research, 103(B3), 5225–5239.

Lin, W., Byrne, T. B., Kinoshita, M., Mcneill, L. C., Chang, C., Lewis, J. C., Yamamoto, Y., et al. (2016), Distribution of stress state in the Nankai subduction zone, southwest Japan and a comparison with Japan Trench. *Tectonophysics*, *692*, 120–130. https://doi.org/10.1016/j.tecto.2015.05.008

Lin, W., Conin, M., Moore, J. C., Chester, F. M., Nakamura, Y., Mori, J. J., Anderson, L., et al. (2013), Stress State in the Largest Displacement Area of the 2011 Tohoku-Oki Earthquake. *Science*, *339*(687). https://doi.org/10.1126/science.1229379

Lin, W., Doan, M. L., Moore, J. C., McNeill, L., Byrne, T. B., Ito, T., et al. (2010), Present-day principal horizontal stress orientations in the Kumano forearc basin of the southwest Japan subduction zone determined from IODP NanTroSEIZE drilling Site C0009. *Geophysical Research Letters*, *37*(13), 1–6. https://doi.org/10.1029/2010GL043158

Lin, W., Yeh, E., Ito, H., Hung, J., Hirono, T., Soh, W., et al. (2007), Current stress state and principal stress rotations in the vicinity of the Chelungpu fault induced by the 1999 Chi-Chi , Taiwan , earthquake. *Geophysical Research Letters*, *34*(L16307). https://doi.org/10.1029/2007GL030515

Litchfield, N. J., Van Dissen, R., Sutherland, R., Barnes, P. M., Cox, S. C., Norris, R., et al. (2014), A model of active faulting in New Zealand. *New Zealand Journal of Geology and Geophysics*, *57*(1), 32–56. https://doi.org/10.1080/00288306.2013.854256

Little, T. A., & Roberts, A. P. (1997), Distribution and mechanism of Neogene to present-day vertical axis rotations , Pacific-Australian plate boundary. *Journal of Geophysical Research*, *102*, 20447–20468.

Ma, K. F., Chan, C. H., & Stein, R. S. (2005), Response of seismicity to Coulomb stress triggers and shadows of the 1999 Mw = 7.6 Chi-Chi, Taiwan, earthquake. *Journal of Geophysical Research*, *110*, B05S19. http://dx.doi.org/10.1029/2004JB003389

Magee, M. E., & Zoback , M. D. (1993), Evidence for a weak interplate thrust fault along the northern Japan subduction zone and implications for the mechanics of thrust faulting and fluid expulsion, *Geology*, *21*, 809–812.

Malinverno, A., Saito, S., & Vannucchi, P. (2016), Horizontal principal stress orientation in the Costa Rica Seis-

mogenesis Project (CRISP) transect from borehole breakouts. *Geochemistry, Geophysics, Geosystems*, *17*(1), 65–77. https://doi.org/10.1002/2015GC006092

McNamara, D. D., Behboudi, E., Wallace, L., Saffer, D. M., Cook, A. E., Fagereng, A., et al (2021), Variable in-situ stress orientations across the northern Hikurangi Subduction Margin. *Geophysical Research Letters*. https://doi.org/10.1029/2020GL091707

Mochizuki, K., Sutherland, R., Henrys, S., Bassett, D., Van Avendonk, H., Arai, R., et al. (2019), Recycling of depleted continental mantle by subduction and plumes at the Hikurangi Plateau large igneous province, southwestern Pacific Ocean. *Geology*, *47*(8), 795–798. https://doi.org/10.1130/G46250.1

Moore, G. F., Boston, B. B., Sacks, A. F., & Saffer, D. M. (2013), Analysis of normal fault populations in the Kumano Forearc Basin , Nankai Trough , Japan : 1 . Multiple orientations and generations of faults from 3-D coherency mapping. *Geochemistry, Geophysics, Geosystems*, *114*, 1989–2002. https://doi.org/10.1002/ggge.20119

Mountjoy, J. J., & Barnes, P. M. (2011), Active upper plate thrust faulting in regions of low plate interface coupling, repeated slow slip events, and coastal uplift: Example from the Hikurangi Margin, New Zealand. *Geochemistry*, *12*(1), Q01005. https://doi.org/10.1029/2010gc003326

Nicol, A., & Beavan, J. (2003), Shortening of an overriding plate and its implications for slip on a subduction thrust, central Hikurangi Margin, *New Zealand. Tectonics*, *22*(6), https://doi.org/10.1029/2003TC001521

Nicol, A., Mazengarb, C., Chanier, F., Rait, G., Uruski, C., & Wallace, L. (2007), Tectonic evolution of the active Hikurangi subduction margin, New Zealand, since the Oligocene. *Tectonics*, *26*(4), 1–24. https://doi.org/10.1029/2006TC002090

Nicol, A., VanDissen, R., Vella, P., Alloway, B., & Melhuish, A. (2002), Growth of contractional structures during the last 10 m.y. at the southern end of the emergent Hikurangi forearc basin, New Zealand. *New Zealand Journal of Geology and Geophysics*, *45*(3), 365–385. https://doi.org/10.1080/00288306.2002.9514979

Pedley, K. L., Barnes, P. M., Pettinga, J. R., & Lewis, K. B. (2010), Seafloor structural geomorphic evolution of the accretionary frontal wedge in response to seamount subduction, Poverty Indentation, New Zealand. *Marine Geology*, *270*(1–4), 119–138. https://doi.org/10.1016/j. margeo.2009.11.006

Peška, P., & Zoback, M. D. (1995), Compressive and tensile failure

of inclined well bores and determination of in situ stress and rock strength. *Journal of Geophysical Research*, *100*(B7), 12791–12811.

Pettinga, J. R. (2004), Three - stage massive gravitational collapse of the emergent imbricate frontal wedge , Hikurangi Subduction Zone , New Zealand. *New Zealand Journal of Geology and Geophysics*, *47*(3), 399–414. https://doi.org/10.1080/00288306.2004.9515066

Rajabi, M., Tingay, M., & Heidbach, O. (2016a), The present-day stress field of New South Wales, Australia. *Australian Journal of Earth Sciences*, *63*(1), 1–21. https://doi.org/10.1080/08120099.2016.1135821

Rajabi, M., Tingay, M., & Heidbach, O. (2016b), The present-day state of tectonic stress in the Darling Basin, Australia: Implications for exploration and production. *Marine and Petroleum Geology*, *77*, 776–790. https://doi.org/10.1016/j.marpetgeo.2016.07.021

Reinecker, J., Tingay, M. R. P., & Müller, B. B. (2003), Borehole breakout analysis from four-arm caliper logs, World Stress Map Project Guidelines World Stress Map Project-Guidelines Four-arm Caliper Logs, 1-5.

Sacks, A., Saffer, D. M., & Fisher, D. (2013), Analysis of normal fault populations in the Kumano forearc basin, Nankai Trough, Japan: 2. Principal axes of stress and strain from inversion of fault orientations. *Geochemistry, Geophysics, Geosystems*, *14*(6), 1973–1988. https://doi.org/10.1002/ggge.20118

Schellart, W. P., & Rawlinson, N. (2013), Global correlations between maximum magnitudes of subduction zone interface thrust earthquakes and physical parameters of subduction zones. *Physics of the Earth and Planetary Interiors*, *225*, 41-67. https://doi.org/10.1016/j.pepi.2013.10.001

Seeber, L., & Armbruster, J.G. (2000), Earthquakes as beacons of stress change. *Nature*, *407*, 69–72.

Stein, R. S. (1999), The role of stress transfer in earthquake occurrence. *Nature*, *402*, 605–609.

Tingay, M., Reinecker, J., & Müller, B. (2008), Borehole breakout and drilling-induced fracture analysis from image logs. World Stress Map Project-Guidelines: Image Logs, 1-8.

Tobin, H., Kinoshita, M., Ashi, J., Lallemant, S., Kimura, G., Screaton, E., et al. (2009), NanTroSEIZE Stage 1 expeditions : introduction and synthesis of key results. In *Proceedings of the Integrated Ocean Drilling Program: 314/315/31.* https://doi.org/10.2204/iodp.proc.314315316.101.2009

Townend, J., & Zoback, M. D. (2006), Stress, strain, and mountain

building in central Japan. *Journal of Geophysical Research: Solid Earth*, *111*(3), 1–11. https://doi.org/10.1029/2005JB003759

Townend, J., Sherburn, S., Arnold, R., Boese, C., & Woods, L. (2012), Three-dimensional variations in present-day tectonic stress along the Australia-Pacific plate boundary in New Zealand. *Earth and Planetary Science Letters*, 353–354, 47–59. https://doi.org/10.1016/j.epsl.2012.08.003

Vavryčuk V. (2015), Earthquake Mechanisms and Stress Field. In: *Beer M., Kougioumtzoglou I., Patelli E., Au IK. (Eds) Encyclopedia of Earthquake Engineering.* Springer, Berlin, Heidelberg. https://doi.org/10.1007/978-3-642-36197-5_295-1

Walcott, R. I. (1987), Geodetic strain and the deformation history of the North Island of New Zealand during the late Cainozoic. Philosophical Transactions of the Royal Society of London. Series A, *Mathematical and Physical Sciences*, *321*, 163-181.

Wallace, L. M. (2020), Slow Slip Events in New Zealand. *Annual Review of Earth and Planetary Sciences*, 1–29.

Wallace, L. M., & Beavan, J. (2010), Diverse slow slip behavior at the Hikurangi subduction margin, New Zealand. *Journal of Geophysical Research: Solid Earth*, *115*(12), 1–20. https://doi.org/10.1029/2010JB007717

Wallace, L. M., & Eberhart-Phillips, D. (2013), Newly observed, deep slow slip events at the central Hikurangi margin, New Zealand: Implications for downdip variability of slow slip and tremor, and relationship to seismic structure. *Geophysical Research Letters*, *40*(20), 5393–5398. https://doi.org/10.1002/2013gl057682

Wallace, L. M., Beavan, J., Bannister, S., & Williams, C. (2012a), Simultaneous long-term and short-term slow slip events at the Hikurangi subduction margin , New Zealand : Implications for processes that control slow slip event occurrence, duration, and migration. *Journal of Geophysical Research*, *117*(B11402). https://doi.org/10.1029/2012JB009489

Wallace, L. M., Beavan, J., McCaffrey, R., & Darby, D. (2004), Subduction zone coupling and tectonic block rotations in the North Island, *New Zealand. Journal of Geophysical Research: Solid Earth*, *109*(12), 1–21. https://doi.org/10.1029/2004JB003241

Wallace, L. M., Fagereng, Å., & Ellis, S. (2012b), Upper plate tectonic stress state may infl uence interseismic coupling on subduction megathrusts. *Geology*, *40*(10), 895–898. https://doi.org/10.1130/G33373.1

Wenning, Q. C., Berthet, T., Ask, M., Zappone, A., Rosberg, J. E., & Almqvist, B. S. G. (2017), Image log analysis of in situ stress orientation, breakout growth, and natural geologic structures to 2.5 km depth in central Scandinavian Caledonides: Results from the COSC-1 borehole. *Journal of Geophysical Research: Solid Earth*, *122*(5), 3999–4019. https://doi.org/10.1002/2016JB013776

Western Energy New Zealand. (2001), Well Completion Report Kauhauroa-4B, Ministry of Economic Development New Zealand, Unpublished Open file Petroleum Report 2610.

Williams, C. A., Eberhart-Phillips, D., Bannister, S., Barker, D. H. N., Henrys, S., Reyners, M., & Sutherland, R. (2013), Revised interface geometry for the hikurangi subduction zone, *New Zealand. Seismological Research Letters*, *84*(6), 1066–1073. https://doi.org/10.1785/0220130035

Wu, H., Kinoshita, M., & Sanada, Y. (2012), Stress state estimation by geophysical logs in NanTroSEIZE Expedition 319-Site C0009, Kumano Basin , southwest Japan. *Geophysical Research Letters*, *39*(L18303). https://doi.org/10.1029/2012GL053086

Zal, H. J., Jacobs, K., Savage, M. K., Yarce, J., Mroczek, S., Graham, K., et al. (2020), Temporal and spatial variations in seismic anisotropy and VP/VS ratios in a region of slow slip. *Earth and Planetary Science Letters*, *532*, 115970. https://doi.org/10.1016/j.epsl.2019.115970

Zoback, M. D. (2007), Reservoir Geomechanics. Cambridge University Press.

Zoback, M. D., Zoback, M. L., Eaton, J. P. , Mount, V. S. & Suppe, J. (1987), New evidence on the state of stress of the San Andreas Fault, *Science, 238*, 1105–1111. https://doi:10.1126/science.238.4830.1105.